

Doctoral Dissertation
Doctoral Program in Metrology (34.th cycle)

A new setup and methods for the fast production of ultracold atoms for atom-ion experiments

Federico Berto

* * * * *

Supervisor
Dr. C. Sias, Supervisor

Politecnico di Torino

I hereby declare that, the contents and organisation of this dissertation constitute my own original work and does not compromise in any way the rights of third parties, including those relating to the security of personal data.

.....

Federico Berto

Turin,

Chapter 5

Single photon sideband cooling in state-dependent potentials

In this chapter a novel scheme for cooling particles confined in optical potentials is presented. A mathematical model describing the vibrational state of motion of particles trapped in state-dependent non-harmonic optical potentials is developed and used to study different atomic species. An efficient cooling method is proposed to reduce the particle's energy by exciting its motional sidebands.

In section 5.1 an overview of sideband cooling in state-dependent optical potentials is presented. The mathematical model is described in section 5.2. Starting from *ab initio* considerations a master rate equation governing the occupation probabilities of the trap bound levels is obtained. In section 5.3 a numeric solution for sideband cooling of a Two-Level System (TLS) trapped in optical tweezers is presented. In section 5.4 the model is used to study cooling of Li atoms trapped in a cavity-enhanced optical lattice. The cavity parameters are chosen to be the same of the high-finesse optical resonator installed in the MOT chamber presented in chapter 4.

Part of the work presented in this chapter was published in ref. [193].

5.1 Sideband cooling in optical potentials

An overview of sideband cooling for particles trapped in harmonic potentials and the assumptions behind that model were presented in section 2.1.5. These assumptions are seldom verified when describing particles trapped in optical potentials. First, optical potentials are rarely deep enough to be well approximated as harmonic. Therefore, the actual shape of the trap has to be taken into account. Second, the potential depth generated by a light field is proportional to the atomic polarizability $\alpha(\omega)$, where ω is the light field frequency. Generally, different electronic configurations of the atom have a different polarizability response, in practice

the potential experienced by the atom in its internal ground state can be different from the potential experienced when it is in its internal excited state. In this case one refers to the optical trap as being *state-dependent*.

To avoid the issue of working in state-dependent potentials, it is possible to make use of traps operating at the so-called "magic" wavelengths. These are wavelength values for which the polarizabilities of the ground ($\alpha_g(\omega)$) and excited ($\alpha_e(\omega)$) states involved in the cooling transition are equal. Unfortunately, for many atomic species the exact values of the magic wavelengths are either not precisely determined or experimentally difficult to achieve. A second option is performing sideband cooling using two-photon Raman transitions. With this method the levels used for cooling can be two sublevels (*e.g.* hyperfine or Zeeman) of the electronic ground state manifold [194] that experience the same trapping potential. Even so, being able to perform single photon sideband cooling remains an attractive proposition as the method is in principle faster (higher scattering rate) and technically simpler (only one laser light is needed).

A semiclassical model for sideband cooling of a TLS in a state-dependent harmonic potential was developed by ref. [195]. The authors conclude that cooling occurs mainly via the difference in the potential energy accumulated during the motion by a particle in the internal ground or excited state, *i.e.* a "Sisyphus-like" effect that is independent of the momentum transfer between the particle and the photons. Cooling is shown to occur only under the condition of $\alpha_g \leq \alpha_e$, while heating is predicted in the opposite case $\alpha_g > \alpha_e$.

However, a recent experimental study [196] observed that, in the case of $\alpha_g > \alpha_e$, cooling is still possible using a laser blue detuned with respect to the free atom transition frequency. The blue detuned laser acts as a "Sisyphus cap", *i.e.* a particle is resonant with the cooling transition only when it has potential energy E_{cap}. As a result, a particle with energy $E \leq E_{\text{cap}}$ is cooled until is not resonant with the cooling laser, and a particle with $E > E_{\text{cap}}$ is heated up and eventually lost from the trap. Effectively, the "Sisyphus-like" effect observed is acting as a repeller, *i.e.* when the particle energy is close to a certain critical value it is pushed to either higher or lower energies.

This interpretation suggests a new method for cooling particles to low vibrational states: if the position of the "Sisyphus cap" could be precisely controlled (by controlling the detuning of the cooling laser), it would be possible to gently "push" the particles' energy toward the ground state of motion while minimizing the particle loss. To this end, a mathematical model describing the vibrational state of trapped particles must be developed taking into account the optical potential shape, the difference in polarizability between ground and excited states as well as the time dependence of the cooling laser detuning.

5.2 1D mathematical model

5.2.1 System Hamiltonian

In order to develop the mathematical description of sideband cooling for state-dependent traps a TLS having linewidth γ, mass m, ground state $|g\rangle$, and excited state $|e\rangle$ is considered. The TLS is trapped in a constant non-harmonic potential V with a state-dependent depth $V_{\mathrm{T},j}$, where $j = g, e$ indicates the ground and the excited internal state of the particle, respectively. The only constraint posed on the potential V is that it's a continuos and differentiable function of space, *i.e.* it is a physically realizable potential.

The TLS is coupled to the cooling laser, which has an electric field

$$\boldsymbol{\mathcal{E}}_{\mathrm{c}} = \boldsymbol{\epsilon}\, \mathcal{E}_0^{(\mathrm{c})} \cos(\mathbf{k}_{\mathrm{c}} \cdot \mathbf{r} - \omega_{\mathrm{c}} t)\,,$$

where $\boldsymbol{\epsilon}$ is the light polarization, $\mathcal{E}_0^{(\mathrm{c})}$ the field amplitude, $\mathbf{k}_{\mathrm{c}}$ the laser wavevector, $\mathbf{r}$ is the spatial coordinate, and ω_{c} the laser pulsation. The problem of a particle interacting with an external electromagnetic field can be treated — in the dipole approximation — with two complementary approaches: the so-called *minimal coupling* approach (ref. [60], chapter 11), which consists in substituting the particle momentum $\mathbf{p}$ with $\mathbf{p} - (e/c)\mathbf{A}$, $\mathbf{A}$ being the magnetic vector potential. The second approach is called the *direct coupling* approach, it consists in introducing a perturbation Hamiltonian $H' = -\mathbf{d}\cdot\boldsymbol{\mathcal{E}}$, where $\mathbf{d}$ is the particle's dipole momentum and $\boldsymbol{\mathcal{E}}$ is the electric field. If the electromagnetic field is treated as an external, non-dynamic quantity then the two approaches have been demonstrated to be mathematically equivalent [197]. In direct coupling formalism, the system Hamiltonian is written as

$$H = H_0 + V - \mathbf{d}\cdot\boldsymbol{\mathcal{E}}_{\mathrm{c}} = H_0 + V + H'\,, \tag{5.1}$$

where H_0 represents the Hamiltonian of the unperturbed TLS. To describe the reduction of kinetic energy of the bound particle, it is convenient to transition to the occupation number representation of eq. (5.1) by introducing the number states $|g, n_g\rangle$ and $|e, m_e\rangle$, where g (e) indicates the ground (excited) internal state of the TLS. These states indicate the number of vibrational quanta possessed by the TLS in the internal ground or excited state. Notably, $|n_g\rangle$ and $|m_e\rangle$ are associated with different wavefunctions, since we consider state-dependent potentials.

The complete Fock space is the tensor product of the two subspaces $\{|g, n_g\rangle\} \otimes \{|e, m_e\rangle\}$. For each subspace two different creation and annihilation operators must be introduced: $\hat{b}^\dagger_{n_g}$ ($\hat{b}^\dagger_{m_e}$) and $\hat{b}_{n_g}$ ($\hat{b}_{m_e}$) are the creation and annihilation operators for a vibrational quantum in the spectrum $\{|g, n_g\rangle\}$ ($\{|e, m_e\rangle\}$). All operators follow a bosonic algebra. With these definitions the second-quantization form of

one-particle $\hat{O}(1)$ and two-particle $\hat{O}(2)$ operators is given by (ref. [198], chapter 1)

$$\hat{O}^{(\mathrm{SQ})}(1) = \sum_{i,j} \langle i|\hat{O}(1)|j\rangle \ \hat{b}_i^\dagger \hat{b}_j \,,$$
$$\hat{O}^{(\mathrm{SQ})}(2) = \sum_{i,j}\sum_{i',j'} \langle i,j|\hat{O}(2)|i',j'\rangle \ \hat{b}_i^\dagger \hat{b}_j^\dagger \hat{b}_{i'} \hat{b}_{j'} \,,$$

where the indices i, i', j, j' run over all possible states $\{|g, n_g\rangle\}$ and $\{|e, m_e\rangle\}$. The products $\hat{b}_i^\dagger \hat{b}_j$ can be more conveniently written as the projectors $\hat{P}_{j\to i} = |i\rangle\langle j|$.

In second-quantization form, the first term appearing in eq. (5.1) is

$$\begin{aligned} H_0 &= \sum_{n_g,n_g'} \left\langle g, n_g \middle| H_0 \middle| g, n_g' \right\rangle |g, n_g\rangle \left\langle g, n_g' \right| + \sum_{m_e,m_e'} \langle e, m_e|H_0|e, m_e'\rangle \ |e, m_e\rangle \langle e, m_e'| \\ &= \sum_{n_g,n_g'} E_g \delta_{n_g,n_g'} \ |g, n_g\rangle \left\langle g, n_g' \right| + \sum_{m_e,m_e'} E_e \delta_{m_e,m_e'} \ |e, m_e\rangle \langle e, m_e'| \\ &= E_g |g, n_g\rangle \langle g, n_g| + E_e |e, m_e\rangle \langle e, m_e| \ , \end{aligned} \tag{5.2}$$

where E_g and E_e represent the energies of the TLS internal states. Diagonal terms are not considered since it is assumed that H_0 is diagonal in the $|g\rangle, |e\rangle$ basis. The second term of eq. (5.1) is

$$\begin{aligned} V &= \sum_{n_g,n_g'} \left\langle g, n_g \middle| V \middle| g, n_g' \right\rangle |g, n_g\rangle \left\langle g, n_g' \right| + \sum_{m_e,m_e'} \langle e, m_e|V|e, m_e'\rangle \ |e, m_e\rangle \langle e, m_e'| \\ &= \sum_{n_g,n_g'} E_{n_g} \delta_{n_g,n_g'} \ |g, n_g\rangle \left\langle g, n_g' \right| + \sum_{m_e,m_e'} E_{m_e'} \delta_{m_e,m_e'} \ |e, m_e\rangle \langle e, m_e'| \\ &= E_{n_g} |g, n_g\rangle \langle g, n_g| + E_{m_e} |e, m_e\rangle \langle e, m_e| \ , \end{aligned} \tag{5.3}$$

where E_{n_g} and E_{m_e} represent the energies of the bound levels of the potential experienced by the TLS in its internal ground and excited states of the TLS. Again, V is assumed to be diagonal in the $|n_g\rangle, |m_e\rangle$ basis, thus off-diagonal terms are not considered. The sums of terms in eqs. (5.2) and (5.3) can be conveniently written as

$$H_0 + V = E_{g,n_g} |g, n_g\rangle \langle g, n_g| + E_{e,m_e} |e, m_e\rangle \langle e, m_e|$$

where $E_{g,n_g} = E_g + E_{n_g}$ and $E_{e,m_e} = E_e + E_{m_e}$. Lastly, the coupling term of eq. (5.1) is

$$H' = \sum_{n_g,m_e} \langle e, m_e|H'|g, n_g\rangle \ |e, m_e\rangle \langle g, n_g| + \sum_{n_g,m_e} \langle g, n_g|H'|e, m_e\rangle \ |g, n_g\rangle \langle e, m_e| \ ,$$

where only the non-diagonal terms have been kept since $\langle i|\mathbf{d}|i\rangle = 0$, $i = g, e$. The matrix elements are given by

$$\begin{aligned}\langle e, m_e|-\mathbf{d}\cdot\boldsymbol{\mathcal{E}}_{\mathrm{c}}|g, m_g\rangle &= \frac{e_0}{2}\left\langle e, m_e\middle|\mathbf{r}\cdot\boldsymbol{\epsilon}\,\mathcal{E}_0^{(\mathrm{c})}\left(e^{i(\mathbf{k}_{\mathrm{c}}\cdot\mathbf{r}-\omega_{\mathrm{c}}t)}+e^{-i(\mathbf{k}_{\mathrm{c}}\cdot\mathbf{r}-\omega_{\mathrm{c}}t)}\right)\middle|g, m_g\right\rangle \\ &= \frac{\hbar\Omega}{2}\Big[\,\langle m_e|e^{i\mathbf{k}_{\mathrm{c}}\cdot\mathbf{r}}|n_g\rangle\, e^{-i\omega_{\mathrm{c}}t} + \langle m_e|e^{-i\mathbf{k}_{\mathrm{c}}\cdot\mathbf{r}}|n_g\rangle\, e^{i\omega_{\mathrm{c}}t}\Big]\,,\end{aligned} \tag{5.4}$$

where $\mathbf{d} = -e_0\mathbf{r}$, $\Omega = e_0\mathcal{E}_0/\hbar\,\langle e|\mathbf{r}\cdot\boldsymbol{\epsilon}|g\rangle$ is the Rabi frequency, and e_0 is the signless elementary electric charge. The exponential terms $e^{\pm i\mathbf{k}_{\mathrm{c}}\cdot\mathbf{r}}$ has been approximated as 1 in the integration over $|g\rangle$ and $|e\rangle$, this can be justified by considering that most atomic wavefunctions are confined to just a few nm, while visible and near UV light — commonly used to manipulate atoms — has a wavelength of a few hundreds nm, thus $\mathbf{k}_{\mathrm{c}}\cdot\mathbf{r} \ll 1$. The same approximation cannot be applied in the terms $\langle m_e|e^{-i\mathbf{k}_{\mathrm{c}}\cdot\mathbf{r}}|n_g\rangle$ since these are bound states wavefunction the dimension of which is determined by the potential geometry, which is comparable with the light wavelength. In order to eliminate the time dependency from the interaction Hamiltonian H', the RWA is used to remove the terms oscillating as $e^{i\omega_{\mathrm{c}}t}$ in eq. (5.4), leading to

$$\begin{aligned}H' &= \frac{\hbar\Omega}{2}\left(\sum_{n_g,m_e} M_{n_g,m_e}\, e^{-i\omega_{\mathrm{c}}t}\,|e, m_e\rangle\,\langle g, n_g| + \sum_{n_g,m_e} M^*_{n_g,m_e}\, e^{+i\omega_{\mathrm{c}}t}\,|g, n_g\rangle\,\langle e, m_e|\right) \\ &= \frac{\hbar\Omega}{2}\sum_{n_g,m_e}\left(M_{n_g,m_e}\, e^{-i\omega_{\mathrm{c}}t}\,|e, m_e\rangle\,\langle g, n_g| + M^*_{n_g,m_e}\, e^{+i\omega_{\mathrm{c}}t}\,|g, n_g\rangle\,\langle e, m_e|\right),\end{aligned}$$

with $M_{n_g,m_e} = \langle m_e|e^{i\mathbf{k}_{\mathrm{c}}\cdot\mathbf{r}}|n_g\rangle$. Then, a transformation to a frame of reference rotating at the same frequency ω_{c} as the laser is performed (further mathematical details on the RWA and the rotating frame transformation are given in appendix C). The final form of the interaction Hamiltonian is

$$\begin{aligned}H' =& \frac{\hbar\Omega}{2}\sum_{n_g,m_e}\left(M_{n_g,m_e}\,|e, m_e\rangle\,\langle g, n_g| + M^*_{n_g,m_e}\,|g, n_g\rangle\,\langle e, m_e|\right) \\ &+ \frac{\hbar\omega_{\mathrm{c}}}{2}\left(\sum_{n_g}|g, n_g\rangle\,\langle g, n_g| - \sum_{m_e}|e, m_e\rangle\,\langle e, m_e|\right),\end{aligned}$$

The fully quantized Hamiltonian is then written as

$$\begin{aligned}H =& \sum_{n_g}\left(E_{g,n_g} + \frac{\hbar\omega_c}{2}\right)|g, n_g\rangle\langle g, n_g| + \\ &+ \sum_{m_e}\left(E_{e,m_e} - \frac{\hbar\omega_c}{2}\right)|e, m_e\rangle\langle e, m_e| + \\ &+ \frac{\hbar\Omega}{2}\sum_{n_g,m_e}\Big[M_{m_e,n_g}|g, n_g\rangle\langle e, m_e| + M^*_{m_e,n_g}|e, m_e\rangle\langle g, n_g|\Big]\,.\end{aligned} \tag{5.5}$$

An implicit approximation has been introduced when performing the transformation to a rotating frame of reference: the transformation has been performed by assuming the system is a TLS, effectively by modifying only the wavefunction related to the $|g\rangle$ and $|e\rangle$ states. In fact — due to the presence of the bound levels — it is a multi-level system and the rotating frame transformation should take into account the complete wavefunctions $\{|g, n_g\rangle\}$ and $\{|e, m_e\rangle\}$. In principle, it is possible to perform the rotating frame transformation using a more complex rotation matrix [199]. However, the transformation can still be performed approximating the system as a TLS as long as the energy difference $E_{g,n_g+1} - E_{g,n_g}$ remains small compared to $E_e - E_g$, in other words if the trap frequencies are small compared to the resonant laser frequency.

5.2.2 Spontaneous emission and master rate equation

In order to take into account the spontaneous emission, which itself may cause changes in the TLS motional state [200], the open system dynamics have to be taken into account. The most general quantum dynamics[1] for open quantum systems are generated by the Gorini-Kossakowski-Sudarshan-Lindblad equation [201, 202, 203] (often referred to as Lindblad equation)

$$\dot{\rho} = -i[H, \rho] + \sum_j L_j \, \rho \, L_j^\dagger - \frac{1}{2}\Big\{L_j^\dagger \, L_j, \rho\Big\}\,, \tag{5.6}$$

where ρ is the system density matrix, L_j are the decay operators describing the non-coherent collapse of the system wavefunction, and $j = (n_g, m_e)$ runs over all bound states indices. The expression of L_j is [204]

$$L_{m_e,n_g} = \sqrt{\gamma_{m_e,n_g}}\, |g, n_g\rangle\langle e, m_e|\ , \tag{5.7}$$

with rates γ_{m_e,n_g} given by [205]

$$\gamma_{m_e,n_g} = \frac{\gamma}{2} \int_{-1}^{+1} \mathrm{d}u\, N(u) \Big| \langle n_g | e^{iku\hat{z}} | m_e \rangle \Big|^2. \tag{5.8}$$

The integration over u averages over all possible direction of the emitted photon wavevector k weighted by the dipole emission angular distribution $N(u) = 3(1 + u^2)/8$. For $u = \pm 1$ the photon is emitted along the trap axis, in this case the

[1] This assumes that the interaction between the atom and the electromagnetic vacuum can be modelled as a Markovian interaction between a system and a bath. The term "Markovian" entails that the system dynamics and the bath dynamics are separable (no correlations between the two), and that any system perturbation on the bath leaves the bath in thermal equilibrium. Generally, the atom-vacuum interaction fulfils all these assumptions.

momentum transfer is maximal, on the other hand $u = 0$ indicates a photon emitted orthogonal to the trap axis and no change in the motional state can occurs.

Different methods allow for a direct solution of the Lindblad equation, *e.g.* wavefunction Monte Carlo (described in section 5.3.2). However, if the coupling between ground and excited states is weak, *i.e.* the natural decay dynamics is much faster than any other dynamics in the system [206], it is possible to perform an adiabatic elimination of the excited states and obtain a master rate equation describing the occupation of different ground state bound levels. A sufficient condition for this approximation is $\Omega/\gamma \ll 1$, *i.e.* the cooling laser must have a relatively low intensity.

The adiabatic elimination is performed following the procedure presented by Reiter and Sørensen [207]. The Hamiltonian in eq. (5.5) can be written as the sum of 4 terms

$$H = H_g + H_e + V_+ + V_- \,,$$

where

$$\begin{aligned}
H_g &= \sum_{n_g} \left(E_{g,n_g} + \frac{\hbar\omega_c}{2} \right) |g, n_g\rangle\langle g, n_g| \,, \\
H_e &= \sum_{n_g} \left(E_{e,m_e} - \frac{\hbar\omega_c}{2} \right) |e, m_e\rangle\langle e, m_e| \,, \\
V_- &= \frac{\hbar\Omega}{2} \sum_{n_g, m_e} M^*_{m_e,n_g} \, |g, n_g\rangle\langle e, m_e| \,, \\
V_+ &= \frac{\hbar\Omega}{2} \sum_{n_g, m_e} M_{m_e,n_g} \, |e, m_e\rangle\langle g, n_g| \,.
\end{aligned}$$

Th term H_g (H_e) describes the dynamic evolution of the ground (excited) states. The perturbative excitation (de-excitation) term V_+ (V_-) includes all terms proportional to projectors of the form $|e, m_e\rangle \langle g, n_g|$ ($|g, n_g\rangle \langle e, m_e|$). The adiabatic elimination is performed by introducing the *effective* Hamiltonian (H_{eff}) and decay operators ($L^{\text{eff}}_{m_e,n_g}$), that describe the dynamics of the vibrational states associated to the electronic ground state

$$\begin{aligned}
H_{\text{eff}} &= -\frac{1}{2} V_- \left[H_{\text{NH}}^{-1} + \left(H_{\text{NH}}^{\dagger} \right)^{-1} \right] V_+ + H_g \,, \\
L^{\text{eff}}_{m_e,n_g} &= L_{m_e,n_g} H_{\text{NH}}^{-1} V_+ \,,
\end{aligned}$$

where

$$\begin{aligned}
H_{\text{NH}}^{-1} &= (H_{\text{NH}} - E_g - \omega_{\text{c}})^{-1}, \\
H_{\text{NH}} &= H_e - \frac{i}{2} \sum_j L_j^{\dagger} L_j \,.
\end{aligned}$$

It follows that

$$H_{\mathrm{NH}} = \sum_{m_e} \left(E_{e,m_e} - \frac{\hbar\omega_c}{2} - \frac{i}{2}\sum_{n_g} \gamma_{m_e,n_g} \right) |e,m_e\rangle\langle e,m_e| \,,$$
$$H_{\mathrm{NH}}^{-1} = \sum_{n_e} \frac{1}{\Delta_{m_e,n_g} - i\frac{\gamma}{2}} |e,m_e\rangle\langle e,m_e| \,,$$

where $\Delta_{m_e,n_g} = (E_{e,m_e} - E_{g,n_g})/\hbar - \omega_c$. The effective Hamiltonian and decay operators result in

$$H_{\mathrm{eff}} = -\left(\frac{\hbar\Omega}{2}\right)^2 \sum_{n_g,n_g'} \left[\sum_{m_e} \Delta_{m_e,n_g'} \frac{M_{m_e,n_g} M_{n_g',m_e}}{\Delta_{m_e,n_g'}^2 + \frac{\gamma^2}{4}} \right] \left|g,n_g\right\rangle\!\left\langle g,n_g'\right| + \sum_{n_g} E_{g,n_g} |g,n_g\rangle\langle g,n_g| \,,$$
$$L_{\mathrm{eff}}^{(n_g,m_e)} = \sqrt{\gamma_{n_g,m_e}} \frac{\hbar\Omega}{2} \sum_{n_g'} \frac{M_{n_g',m_e}}{\Delta_{m_e,n_g'} - i\frac{\gamma}{2}} \left|g,n_g\right\rangle\!\left\langle g,n_g'\right| \,. \tag{5.9}$$

To describe the dynamics of the ground state, the Lindblad equation (eq. (5.6)) is re-written in terms of the effective operators (eq. (5.9))

$$\dot{\rho} = -i[H_{\mathrm{eff}},\rho] + \sum_{n_g,m_e} L_{\mathrm{eff}}^{(n_g,m_e)} \rho \left(L_{\mathrm{eff}}^{(n_g,m_e)}\right)^\dagger - \frac{1}{2}\left\{ \left(L_{\mathrm{eff}}^{(n_g,m_e)}\right)^\dagger L_{\mathrm{eff}}^{(n_g,m_e)}, \rho \right\} .$$

Finally, if one considers the diagonal elements $\Pi_{n_g} = \langle g,n_g|\rho|g,n_g\rangle$, the expectation value of the commutator $[H_{\mathrm{eff}},\rho]$ is zero, and the other terms yield

$$\begin{aligned} \dot{\Pi}_{n_g} = &- \sum_{m_e,n_g'} \left|\gamma_{m_e,n_g'}\right| \left|M_{n_g,m_e}\right|^2 \Gamma\left(\Delta_{m_e,n_g}\right) \Pi_{n_g} \\ &+ \sum_{n_g'} \left(\sum_{m_e} \left|\gamma_{m_e,n_g}\right| \left|M_{n_g',m_e}\right|^2 \Gamma\left(\Delta_{m_e,n_g'}\right) \right) \Pi_{n_g'} \,, \end{aligned} \tag{5.10}$$

where $\Gamma(\Delta) = (\Omega/2)^2/(\Delta^2 + \gamma^2/4)$ is the scattering rate function.

The first, negative term on the right-hand side of eq. (5.10) represents the loss of population from the state $|g,n_g\rangle$ due to transitions to the excited states $|e,m_e\rangle$ followed by spontaneous decay to $\left|g,n_g'\right\rangle$, while the second term represents the increase of the $|g,n_g\rangle$ population due to an absorption-spontaneous emission cycle starting from the $\left|g,n_g'\right\rangle$ level.

To generalize the model to a multilevel system, in particular to the hyperfine structure of an atom, one can perform the following substitutions in eq. (5.10): $n_g \to (F_g, m_{F_g}, n_g)$, $m_e \to (F_e, m_{F_e}, m_e)$ and $n_g' \to (F_g', m_{F_g}', n_g')$, where F_g (F_e) and m_{F_g} (m_{F_e}) denote different hyperfine states of the ground (excited) state manifold of the atom. In general γ and Ω will also depend on the particular (F_g, m_{F_g}), (F_e, m_{F_e}) combination considered via the associated transition line strengths [109].

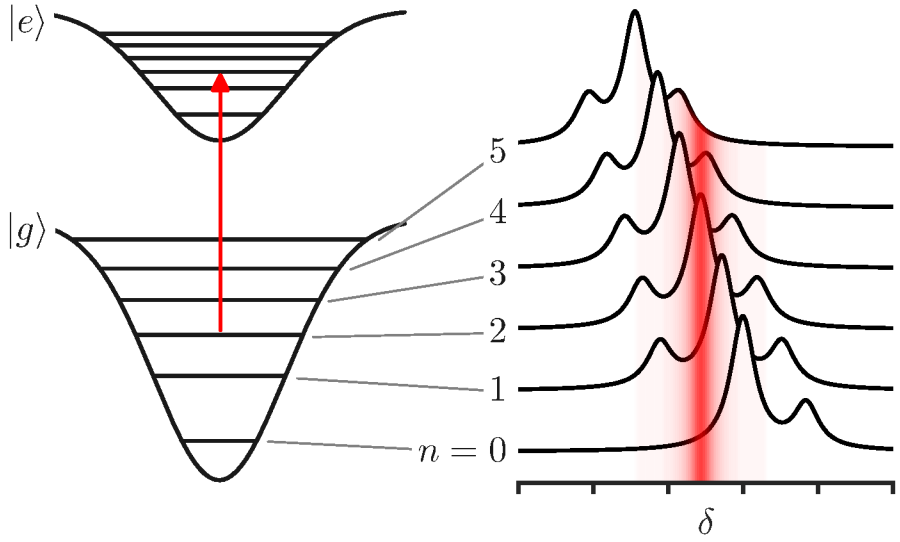

Figure 5.1: (Left) Sketch of the trap potential for ground ($|g\rangle$) and excited ($|e\rangle$) states. The red arrow indicates the position of a laser resonant with the $|g, 2\rangle \rightarrow |e, 2\rangle$ transition. (Right) Sketch of the spectrum of a particle confined in a state-dependent optical potential (with $|V_{\mathrm{T},g}| > |V_{\mathrm{T},e}|$). The red halo indicates the frequency region of high scattering rate from a laser resonant with the $|g, 2\rangle \rightarrow |e, 2\rangle$ transition.

The matrix elements M_{n_g,m_e} determine how different bound states are coupled by the cooling laser beam. The exponential term can be expanded to the first order Taylor series

$$\langle n_g|e^{ik\hat{z}}|m_e\rangle \approx I_{m_e,n_g} + ik\,\langle n_g|\hat{z}|m_e\rangle + \mathcal{O}\Big((kz)^2\Big)\,.$$

For the purpose of this explanation the potential is assumed harmonic, and the overlap integrals $I_{m_e,n_g} = \langle n_g|m_e\rangle$ are approximated by a Kronecker delta δ_{n_g,m_e}. Under this assumption

$$\langle n_g|e^{ik\hat{z}}|m_e\rangle \approx \delta_{m_e,n_g} + i\,\eta\left[(m_e+1)\,\delta_{m_e+1,n_g} + m_e\,\delta_{m_e-1,n_g}\right],$$

where η is the Lamb-Dicke parameter (as defined in section 2.1.5), which is assumed to be much smaller than 1. Therefore, under the harmonic approximation, the particle spectrum presents a *carrier* transition of relative intensity 1 which does not change the motional quantum number and two additional *sideband* transitions which are associated to a change of a single vibrational quantum. These sideband transitions are referred to as the *red sideband* and *blue sideband* and are associated with the loss and gain of a vibrational quantum, respectively. The sideband transitions have a relative intensity η^2. Beyond the harmonic approximation, the matrix elements $\langle n_g|e^{ik\hat{z}}|m_e\rangle$ can be calculated numerically. Also in this case, the

spectrum presents three transitions: the carrier and the two sidebands. Sideband transitions of higher order ($|m_e - n_g| > 1$), contribute to the elements $\langle n_g|e^{ik\hat{z}}|m_e\rangle$ with terms of order $\mathcal{O}(\eta^2)$ or higher. Therefore, they can be neglected as long as $\eta \ll 1$.

The position of the carrier and sideband transitions are given by the Lorentzian function $\Gamma\left(\Delta_{m_e,n_g}\right)$, which is peaked at $\Delta_{m_e,n_g} = 0$, thus the positions of the sideband and the carrier transitions depend on the particular choice of m_e and n_g. The particle absorption spectrum is sketched in fig. 5.1. The configuration of this spectrum shows the Sisyphus-cap effect introduced by ref. [196]: a laser beam resonant with the $|g, n_g\rangle$ carrier transition will cause excitation of the blue sidebands of levels with number $n' > n$, thus causing heating. Contrarily, the same laser will be resonant with the red sidebands of levels with $n' < n$ and, resulting in a reduction of the vibrational level.

The work developed in this chapter aims at studying the possibility of realizing a novel scheme for cooling particles confined in state-dependent optical potentials with $\alpha_g < \alpha_e$. In this scheme a laser is first made resonant with the free space TLS transition ($\Delta = 0$) and then slowly detuned toward the blue side ($\Delta > 0$). This way, the laser becomes resonant with the red sideband of all bounds levels, from the least to the most bound one. Effectively, the laser cools the bound levels sequentially, avoiding scattering on the blue sideband of levels which are still populated. In the following sections, the efficiency of this cooling scheme is investigated in the specific cases of Li and Yb trapped in optical tweezers and optical lattices.

5.3 Sideband cooling of TLS in optical tweezers

Optical tweezers have become common tools for manipulating single atoms, single molecules, or ions [208, 133, 209] with the aim of isolating individual particles. In this section, the cooling scheme proposed at the end of the previous paragraph is applied to two-level particles trapped in optical tweezers. Dipolar traps, such as optical tweezers, constitute a simple case to study since they are formed by a single laser beam. The trap depth and trap frequencies can be independently controlled, since laser power and trap waist are independent parameters. The different case of a cavity-enhanced lattice will be considered in the next section.

A numeric simulation of eq. (5.10) was performed by considering two separate TLSs trapped in an optical tweezer generated by a highly focused single beam laser. In order to perform two simulations under different but still experimentally feasible conditions, the simulation was performed for two TLSs with considerably different mass and spectroscopic properties. Specifically, the two TLSs have the transition frequencies and the masses of Li and Yb. With respect to Yb, the two-level approximation is particularly well suited for the bosonic isotopes for which there is no hyperfine splitting.

Parameter	**Li**	**Yb**
Transition line	$^2S_{1/2} \rightarrow {}^2P_{1/2}$	$^1S_0 \rightarrow {}^3P_1$
λ	1064 nm	532 nm
w_0	700 nm	700 nm
P	47.5 mW	25.8 mW
s_0	0.1	0.1
Ω	8.15×10^6 rad/sec	2.56×10^5 rad/sec
τ	3.3 ms	110 ms
γ	2π 5.8 MHz [165]	2π 182 kHz [210]
m	6 u	171 u
α_g	270 a.u.	280 a.u. [211]
α_e	191 a.u.	224 a.u. [211]

Table 5.1: Parameters used for simulating sideband cooling of a TLS trapped in an optical tweezer. Parameters λ, w_0 and P are the wavelength, waist and power of the optical tweezer's laser beam, respectively. s_0 is the intensity of the cooling laser in units of I_{sat} and τ is the duration of the cooling laser frequency sweep. The last four parameters are the linewidth, mass and polarizabilities of the TLS. u is the atomic mass unit.

Table 5.1 shows the parameters used in the simulation and the properties of the transitions that were considered. The trap wavelength λ, waist w_0, and power P were set to values similar to the ones used in experiments reported in literature [212, 213]. The cooling laser relative intensity $s_0 = I/I_{\text{sat}}$, where I_{sat} is the saturation intensity of the atomic transition, is chosen to be 0.1. Due to the direct relation between s_0 and the ratio Ω/γ this ensures that the condition $\Omega/\gamma \ll 1$ is satisfied. The terms α_g and α_e are the atomic polarizabilities for the ground and the excited states, respectively, and were computed following the method presented in [214]. To convert from atomic units to SI units, α_g and α_e have to be multiplied by $2\pi\hbar \times 2.488\,32 \times 10^{-8}\,\text{A}^2\text{s}^4/\text{kg}$.

Although not strictly necessary, it is convenient to define some approximated quantities which are commonly used in the experimental field when referring to sideband cooling. The equivalent harmonic trapping frequency is defined as

$$\omega_{\text{T},i} = \frac{1}{w_0}\sqrt{2\frac{|V_{\text{T},i}|}{m}}\,, \quad i = g, e$$

where

$$V_{\text{T},i} = \alpha_i \frac{I(x,y,z)}{2\epsilon_0 c}\,, \quad i = g, e$$

is the trap's potential depth when the TLS is in its ground (g) or excited (e) state, $I(x, y, z)$ is the intensity distribution of the trap's laser beam — typically, $I(x, y, z)$ has a Gaussian shape if the laser is emitting in its fundamental mode — ϵ_0 is the vacuum permittivity. It is possible to define a Lamb-Dicke parameter for the ground state manifold as

$$\eta_g = \frac{2\pi}{\lambda_c}\sqrt{\frac{\hbar}{2m\omega_{T,g}}}\,. \tag{5.11}$$

The simulation outcomes are discussed in terms of the approximated parameters $\omega_{T,g}$ and η_g. The values of power P reported in table 5.1 are chosen such that the ground state Lamb-Dicke parameter η_g is equal to 0.2. Since the laser frequency is swept between two values — these will be defined later in the text — the parameter τ indicates the time it takes the cooling laser to perform the sweep. The values of the parameter τ were chosen to be 3.3 ms (Li) and 110 ms (Yb). In the visualization of the simulation results, the time is expressed in units of $\eta_g^2\gamma t$, as this represents the sideband effective scattering rate [200].

Parameter	**Li**	**Yb**
$V_{T,g}$	3.7 mK	2.1 mK
$V_{T,e}$	2.6 mK	1.7 mK
$\omega_{T,g}$	732 kHz	101 kHz
$\omega_{T,e}$	617 kHz	90 kHz
η_g	0.2	0.2
$\Delta\alpha$	−17 %	−11 %

Table 5.2: Physical parameters of the trap used in the sideband cooling simulation.

Table 5.2 shows the physical parameters of the trap computed using the parameters reported in table 5.1. The differential polarizability $\Delta\alpha = (\alpha_e - \alpha_g)/(\alpha_e + \alpha_g)$ indicates of the relative difference in atomic polarizability between the ground and the excited states. A negative value of $\Delta\alpha$ implies $V_{T,g} > V_{T,e}$. For both atomic species the equivalent harmonic trapping frequency $\omega_{T,g}$ is smaller than the transition linewidth γ. The condition $\omega_{T,g} > \gamma$ is required to be able to resolve the sideband transitions from the carrier transition, thus achieving ground state cooling. However, it will be shown in next sections that it is still possible to achieve a reduction of the trapped particles' energy of motion even if $\omega_{T,g} \lesssim \gamma$.

5.3.1 Numerical simulation of sideband cooling

Equation (5.10) is a matrix first-order differential equation of the form

$$\dot{\mathbf{\Pi}} = \mathbf{C} \cdot \mathbf{\Pi}\,,$$

where $\mathbf{C}$ is the coefficient matrix and $\mathbf{\Pi}$ is a column vector, the elements of which are the populations Π_{n_g}. If $\mathbf{C}$ is time-independent, the general solution is a linear combination of eigenvectors of $\mathbf{C}$. Since the coefficients appearing in eq. (5.10) are not time-independent, a dense partition of time is introduced and $\mathbf{C}$ is approximated as constant over each (small) time interval. Therefore, the solution is given by diagonalizing $\mathbf{C}$ over each time interval. A simulation code was developed using the Python language, with the aim of determining the matrix elements of $\mathbf{C}$ while the laser frequency is swept linearly in time.

Initialization and preliminary calculations

Before the $\mathbf{C}$ matrix can be determined, several preliminary calculations have to be performed in order to determine the bound levels energies and wavefunctions starting from the parameters listed in table 5.1. First, a single beam optical trap (optical tweezer) is considered. The trap's laser intensity is given by the formula (ref. [168], chapter 2)

$$I(x,y,z) = I_0 \left| \frac{w_0}{w(z)} H_0\left(\sqrt{2}\frac{x}{w(z)}\right) e^{-(x/w(z))^2} H_0\left(\sqrt{2}\frac{y}{w(z)}\right) e^{-(y/w(z))^2} \right|^2 ,$$

where $I_0 = 2P/(\pi w_0^2)$ is the peak intensity, w_0 is the beam waist, $w(z)$ is the $1/e^2$ radius at position z so that $w(z=0) = w_0$, $H_0(x)$ is the zero-th order Hermite polynomial, the trapping laser propagates along the z-axis, and the phase term has been omitted. The trap depth is computed as [215]

$$V_{\mathrm{T},i}(x,y,z) = -\frac{1}{2\epsilon_0 c} \mathrm{Re}\{\alpha_i\} I(x,y,z), \quad i = g, e$$

Since the potential $V_{\mathrm{T},i}(x,y,z)$ is Gaussian, a numeric method is needed to compute the trap bound levels and wavefunctions. A well-known approximation method for bound states is the *WKB* approximation (ref. [60], chapter 8): the energy of the n-th bound level $E = E_n$ has a value such that

$$n + \frac{1}{2} = \frac{\sqrt{2m}}{\pi\hbar} \int_{R_-}^{R_+} \sqrt{E - V(r)}\, \mathrm{d}r \ , \tag{5.12}$$

where $V(r)$ is the potential energy, $R_\pm$ are the classical inversion points where the particle's total energy equals the potential energy. In code, the WKB integral is computed as a summation over dense partition of space r, the energy of each bound levels is found by solving eq. (5.12) as a root finding problem. The n-th bound state wavefunctions are approximated by the n-th harmonic oscillator wavefunction that best approximates the curvature of the potential at energy E_n. Due to numerical limitations, the simulation works on a truncated basis of 60 bound levels for each of the ground state and excited state manifold, for a total of 120 states simulated.

Matrix elements derivation and simulation main loop

The off-diagonal elements of the matrix **C** are given by

$$C_{n_g,h_g} = \sum_{m_e} \left|\gamma_{m_e,n_g}\right| \left|M_{h_g,m_e}\right|^2 \Gamma\left(\Delta_{m_e,h_g}\right),$$

as indicated in eq. (5.10). Each of the three multipliers appearing in the expression of C_{n_g,h_g} is computed and stored in a temporary matrix. The decay rate γ_{m_e,n_g} is computed as $\gamma/2(|\langle n_g|m_e\rangle|^2 + 7/16\,|ik\,\langle n_g|\hat{z}|m_e\rangle|^2)$, additional terms are neglected, the value $7/16$ is a numeric approximation of the integral over u presented in eq. (5.8). These values are stored in a matrix called *decay_couplings*. The matrix elements M_{h_g,m_e} are computed using the expression $\langle n_g|m_e\rangle + ik\,\langle n_g|\hat{z}|m_e\rangle$ and are stored in a matrix called *couplings*. The scattering rate $\Gamma\left(\Delta_{m_e,h_g}\right)$ is computed from the expression of the Lorentzian function $\Gamma(\Delta) = (\Omega/2)^2/(\Delta^2 + \gamma^2/4)$ and the values are stored in the *scatrates* matrix. These three temporary matrices are organized such that the element at the n-th row and m-th column corresponds to the appropriate rate between the n-th ground state bound level and the m-th excited state bound level. All overlap integrals, such as $\langle n_g|m_e\rangle$, are computed numerically.

Once these three matrices are defined, the matrix **C** is computed with the following code:

```
#
# Computes the matrix C for sideband cooling simulation.
#

# N: number of bound states in ground state manifold

def compute_matrix(laser_frequency):
    # scattering rates for a given laser frequency
    scatrates = compute_scatrates(laser_frequency)
    # create an (NxN) empty matrix
    C = [[0.0]*N for _ in range(N)]

    for ng in range(N):
        for mg in range(N):
            # diagonal terms are computed separately
            if ng == mg:
                continue
            # matrix element
            rate = np.sum(
                decay_couplings[ng] * \
                couplings[mg] * \
                scatrates[mg]
```

```
23              )
                C[ng][mg] += rate
25
    # convert to np.array
27  C = np.array(C, dtype=np.float64)
    # diagonal terms are the sum of other rates
29  # on the same row, with negative sign
    C -= np.diag(np.sum(C, axis=0))
31  # clean small values (limits numeric noise)
    C[np.abs(C) <= 1e-10] = 0.0
33
    return C
```

Since the off-diagonal elements in the n-th row represent the rate of transition from the n-th level all other bound levels with vibrational number different from n and since the sum of all the rates has to be zero (conservation of probability), the diagonal elements of the matrix $\mathbf{C}$ are computed as the sum of the rates on the same row multiplied by -1.

The main loop of the simulation is concerned with changing the laser frequency value over time and re-calculating the matrix $\mathbf{C}$, diagonalizing it at every time interval δt and returning a list of occupation probabilities Π_n. The code of the main loop is:

```
#
2 # Computes the list of occupation probabilities
  # over a partition of time.
4 #

6 # dt: time step between each solution.
  # f0: start frequency for the laser sweep.
8 # f1: stop frequency for the laser sweep.
  # tau: time taken to sweep from f0 to f1.
10 # p0: starting occupation probability.

12 # list of occupation probabilities
  pns = [p0]
14
  while t < tmax:
16    # increase time
      t += dt
18    # compute laser frequency
      f = f0 + (f1-f0)/tau * t
20    # compute C matrix
      C = compute_matrix(laser_frequency = f)
22    # diagonalize
```

```
    eigvals, eigvects = np.linalg.eig(C)
24  c = np.linalg.inv(eigvects) @ pns[-1]
    pn = eigvects @ (c * np.exp(eigvals * dt))
26  # store result
    pns.append(pn)
```

The output of the simulation is the list *pns*, which contains the occupation probabilities for all levels at different times. These can be used to compute other quantities of interests such as the average occupation number $\langle n(t)\rangle$ or the average particle's energy. The variables f_0 and f_1 determine the initial and final frequency of the cooling laser, f_0 corresponds to the free-space (unperturbed) TLS transitions frequency, while the final frequency f_1 is carefully adjusted to minimize the resulting average occupation number $\langle n(t)\rangle$. The optimization is done as follows: a first simulation is performed by setting f_1 equal to the frequency of the $n_g = 1 \rightarrow m_e = 0$ red sideband; when the cooling laser reaches this value, since the sidebands are not well resolved from carrier transitions, heating occurs and the value of $\langle n(t)\rangle$ suddenly increases. The frequency value for which $\langle n(t)\rangle$ is at a minimum is then extracted, and a second, independent simulation is performed where f_1 is set to the value that gave the best result for $\langle n(t)\rangle$ in the previous simulation.

5.3.2 Wavefunction Monte Carlo simulation

In order to compute the dynamics described by eq. (5.1) independently of the approximations performed to obtain eq. (5.10), a Wavefunction Monte Carlo (WFMC) simulation of Hamiltonian 5.1 was developed. Such simulation is not afflicted by the adiabatic elimination of excited states and follows a different mathematical approach in solving the Lindblad equation.

The WFMC method is a stochastic method used to simulate the dynamics of open quantum systems. Different, yet similar, algorithms use a wavefunction-based approach to achieve such result and have been developed concurrently and independently by different people [216, 217, 218, 219]. The method developed by Dalibard *et al.* [216] is sometimes referred to as the *quantum jumps approach*. In this approach the system wavefunction is made to evolve according to the Schrödinger equation with a non-Hermitian Hamiltonian[2]

$$H_{\mathrm{NH}} = H - \frac{i\hbar}{2}\sum_j L_j^\dagger L_j \,.$$

The non-Hermitian component of the Hamiltonian causes a variation of the norm

[2]It is interesting to note that this non-Hermitian Hamiltonian is the same as the one used in section 5.2 to perform the adiabatic elimination of excited states.

of the wavefunction, such that after a small time δt the quantity

$$\delta p = \delta t \sum_j \langle \psi(t) | L_j^\dagger L_j | \psi(t) \rangle$$

indicates the probability that a quantum jump occurred in the time range $t \to t+\delta t$ time. As a result, $\langle \psi(t+\delta t) | \psi(t+\delta t) \rangle = 1 - \delta p$ is the probability of remaining in the state $|\psi\rangle$. When a quantum jump does occur, the wavefunction $|\psi(t)\rangle$ is projected using a Lindblad operator L_j and then normalized to 1

$$\psi(t+\delta t) = \frac{L_j \, |\psi(t)\rangle}{\sqrt{\langle \psi(t) | L_j^\dagger L_j | \psi(t) \rangle}}$$

The collapse operator L_j that performs the measurement is chosen randomly, by weighting each L_j with their associated rate γ_j.

The algorithm for the WFMC is thus:

1. Start from a pure state $|\psi(0)\rangle$.
2. Generate a random number r between 0 and 1.
3. Integrate Schrödinger equation with Hamiltonian H_{NH} until $\langle \psi(t) | \psi(t) \rangle = r$, at this point a quantum jump occurs.
4. Randomly choose a collapse operator L_j weighted by its decay rate. Collapse and normalize the wavefunction.
5. Loop from point 2 until a stop time is reached.

This method defines a so-called *quantum trajectory*, *i.e.* a particular time evolution of the system wavefunction $|\psi\rangle$. This wavefunction can be used to compute quantities of interest, such as expectation values of different operators, which then must be averaged over multiples trajectories. If the initial state is not a pure state but a mixture with probabilities p_n

$$\rho = \sum_n p_n \, |\psi_n(t)\rangle\langle\psi_n(t)| \ ,$$

each trajectory should be initialized with a different $|\psi_n(0)\rangle$ randomly selected according to the distribution of p_n.

The sideband cooling WFMC simulation is implemented using the Python language in the QuTiP framework [220]. This framework implements the algorithm presented above and integrates the wavefunction using the Runge–Kutta–Fehlberg method (RKF45) that solves differential equations with fourth order accuracy and estimates the error with a fifth order accuracy (ref. [221], chapter 17). The simulation parameters are defined as in the beginning of section 5.3. Results are averaged over 250 trajectories.

5.3.3 Results

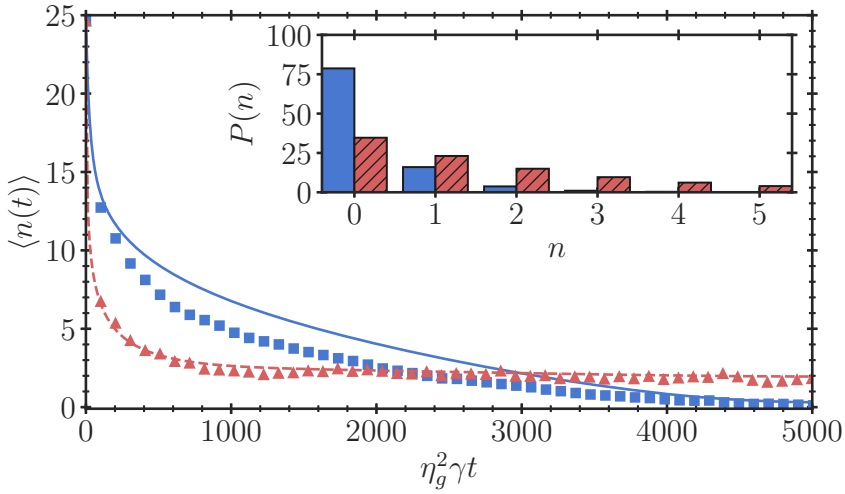

Figure 5.2: Average occupation number as a function of time during sideband cooling of Yb (blue solid line) and Li (red dashed line). The data are obtained by numerical integration of eq. (5.10). The blue squares and the red triangles indicate the results from a quantum Monte Carlo simulation for Yb and Li, respectively. The time axis has been scaled by the sideband scattering rate $\eta_g^2\gamma$. Inset shows the occupation probability of the lowest bound levels after cooling of Yb (blue bars) and Li (red hatched bars) for the analytic result only.

Figure 5.2 shows the results of a single numeric solution of eq. (5.10) as the laser frequency is swept in time. The average occupation number is reduced over time for both Li and Yb atoms, until the particles reach a steady mean energy level. The ground state occupation after the laser sweep is 78.7 % for Yb and 34.6 % for Li, corresponding to an energy reduction of 98.2 % and 92.0 % for the two species, respectively.

In spite of the fact that the product between the red sideband linewidth $\eta_g^2\gamma$ and the laser sweep time are kept equal in the simulation, the dynamic behaviour of the occupation number of Yb and Li is qualitatively different. In particular, Li atoms reach the minimum attainable energy after approx. 1/3 of the sweep time. This discrepancy can be attributed to the different values of the ratio ω_T/γ, which are 0.57 and 0.126 for Yb and Li, respectively. The occupation probability distribution after the cooling process is a thermal distribution (shown inset fig. 5.2), and the associated temperatures are 4.3 µK and 114 µK for Yb and Li, respectively. The WFMC simulation results are shown by the square and triangle markers and qualitatively agree with the numerical solution, according to the WFMC simulation

the ground state occupation probabilities after cooling are 88.0 % for Yb and 38.0 % for Li.

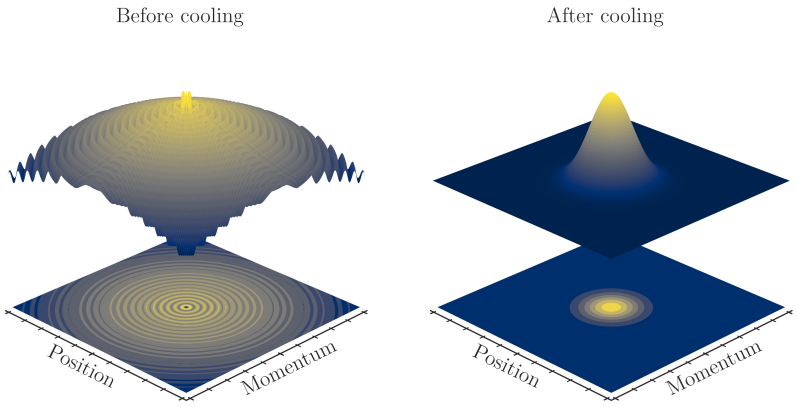

Figure 5.3: Wigner quasiprobability distribution before and after cooling of Yb. Vertical axes have been scaled for better visualisation.

To better visualize the effects of the cooling in phase space, fig. 5.3 shows the Wigner quasiprobability distribution before and after cooling in the case of Yb atoms. The Wigner quasiprobability distribution is a statistical distribution used to describe quantum states in phase space [222], it cannot be strictly interpreted as a probability distribution since it can assume negative values when it describes a state with no classical equivalent. Initially, the atom is broadly spread in phase space (fig. 5.3, left plot) indicating a relatively hot particle. At the end of the laser sweep, the distribution in the phase space is compressed near the origin (fig. 5.3, right plot), showing a reduction of particle momentum and occupied positions, thus demonstrating the cooling of the particle's motion. This final distribution has a Gaussian shape and it is similar to the occupation probability of a Fock state with $n = 0$. Both distributions are centred on the origin as expected for a particle in a symmetric potential.

Since the minimum achievable value for $\langle n(t) \rangle$ is strongly dependent on the choice of the experimental parameters, it is instructive to simulate sideband cooling with varying values for the trap depth, the difference in polarizability and the cooling laser frequency sweep time. Figure 5.4 shows the mean occupation number after cooling for different values of the Lamb-Dicke parameter η_g, which is changed by varying the trap depth. As a result, also the ratio ω_T/γ is varied (top x-axis). As η_g is increased the minimum achievable value for the average occupation number is considerably increased. This is an expected result, since the motional sidebands are less resolved when the condition for the Lamb-Dicke regime is relaxed and the ratio ω_T/γ is increased. The increase of the minimum $\langle n(t) \rangle$ is more pronounced in the case of Li. This can be attributed to the fact that the ω_T/γ ratio is far smaller

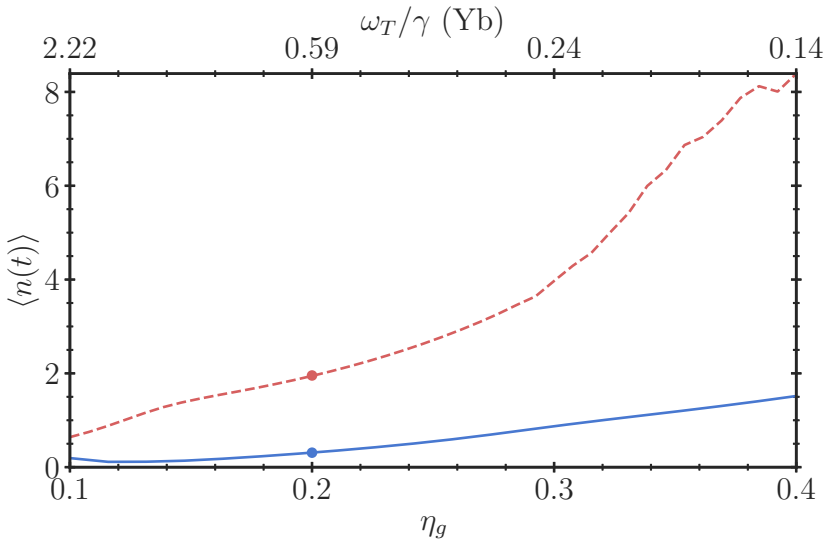

Figure 5.4: Average occupation number after the frequency sweep of the cooling laser as a function of the ground state Lamb-Dicke parameter for Yb (blue solid line) and Li (red dashed line). The x-axis above the plot reports the values of the ratio ω_T/γ for Yb, the corresponding values for Li can be obtained by rescaling the axis by the ratio of the atomic linewidths. Solid dots indicate the parameters used in the simulations of fig. 5.2. Different values of η_g are obtained by changing the trapping laser power.

for Li with respect to Yb due to the different atomic linewidths.

The difference in polarizability determines the difference between the trap depths experienced by an atom in the ground or in the excited internal state. Therefore, this quantity determines the spread of the sidebands' transition frequencies. As the energy difference between the carrier and the sidebands increases, the coupling strength between levels with different motional state decreases, resulting in a lower efficiency of the cooling process. By artificially changing the atomic polarizability of the excited state, the dependence of the minimum achievable occupation number on the difference in polarizability $\Delta\alpha = (\alpha_e - \alpha_g)/(\alpha_e + \alpha_g)$ can be studied. The results of this simulation are shown in fig. 5.5.

As predicted, the further away the system is from the magical trapping condition, the worst is the minimum achievable $\langle n\rangle$. Cooling of Yb is more efficient than Li except for the region where $\Delta\alpha < -0.3$, in which the two curves cross each other and present a similar slope. The fact that at small values of $|\Delta\alpha|$ the Yb $\langle n\rangle$ is smaller than the one of Li is due to the smaller atomic linewidth. For increasing values of $|\Delta\alpha|$ the results for Yb quickly increase since the reduction of the excited state potential depth reduces the resolution between sideband and carrier transitions.

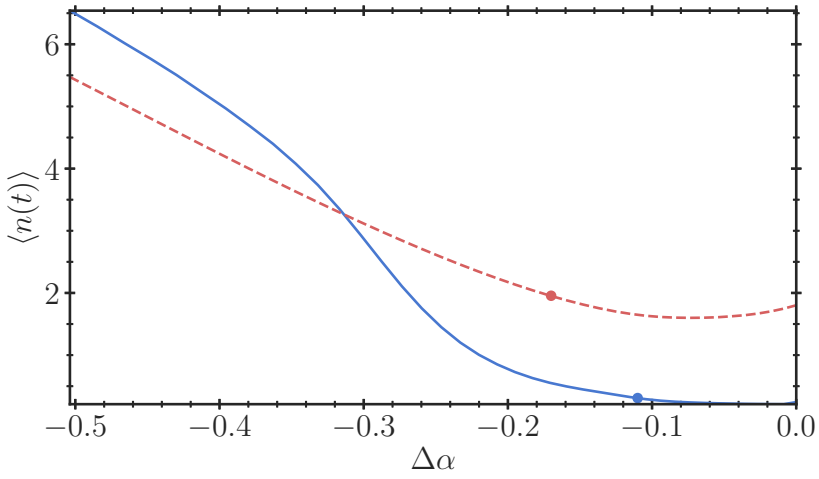

Figure 5.5: Average occupation number after cooling as a function of the difference in polarizability $\Delta\alpha$ for Yb (blue solid line) and Li (red dashed line). $\Delta\alpha = 0$ implies a magic trapping condition, while negative values are associated with a trap for which a particle in its internal ground state is more bound than a particle in the excited state. Solid dots indicate the parameters used in the simulations of fig. 5.2. Different values of $\Delta\alpha$ are obtained by changing the atomic polarizability for the excited state only.

Finally, fig. 5.6 shows the cooling efficiency as a function of the frequency sweep duration when the start and stop frequencies are kept constant. A threshold-like effect is observed if the laser sweep time is gradually reduced. This is due to the fact that, if the laser spends insufficient time at resonance with a given sideband transition, there will be a reduced population transfer between bound levels, which limits the reduction of vibrational quanta.

5.4 Sideband cooling of Lithium in optical lattice

As detailed in chapter 4, a high-finesse optical resonator is installed in the MOT chamber of the Li setup. For an input power of 300 mW the resonator is capable of generating a dipole trap with depths $13\,500 E_{\mathrm{rec}}$ (26.3 mK) and $11\,250 E_{\mathrm{rec}}$ (22.0 mK), where E_{rec} is the recoil energy, for the $^2\mathrm{S}_{\frac{1}{2}}$ and $^2\mathrm{P}_{\frac{1}{2}}$ levels of ^{6}Li, respectively. The trap depth is sufficient to allow for the resolution of sideband transition from carriers, but with a trapping laser wavelength of 903 nm the trap potential is state-dependent.

The dipole trap generated between the resonator mirrors is intended to be used for evaporative cooling after the MOT sequence until the Li cloud is brought to

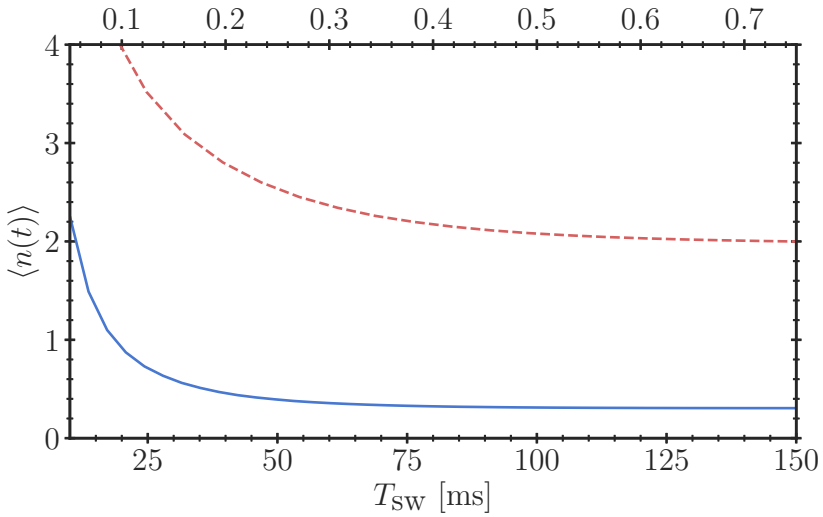

Figure 5.6: Average occupation number after cooling as a function of the sweep duration T_{sw} for Yb (blue solid line) and Li (red dashed line). The lower (upper) axis indicates the sweep duration for Yb (Li).

degeneracy. Single photon sideband cooling can be used to speed up and facilitate this process: instead of starting evaporative cooling with a gas at the temperature of a cMOT ($\approx 40\,\mu\mathrm{K}$), a sideband cooling sequence can be performed before evaporation in order to further reduce the cloud temperature. With this method degeneracy would be reached with a reduced loss of particles and faster, facilitating a higher repetition rate in the experimental run.

The model developed in this work is suitable to describe sideband cooling for particles trapped in optical lattices. Lithium in particular requires to take into account the full Hyperfine Structure (HFS) since the separation between two HFS levels is comparable with the frequency spread of sideband and carriers of different bound states. Therefore, eq. (5.10) is modified to support a multi-level system such as the hyperfine structure of Li as indicated in section 5.2.

The trapping laser polarization is assumed orthogonal to the lattice axis and with a fixed direction (π-polarized light). Under these assumptions, the lattice potential can be written as

$$V_{\mathrm{T},i}(z) = V_{0,i} \cos^2(k_{\mathrm{T}} z)\,, \quad i = g, e \tag{5.13}$$

where $k_{\mathrm{T}} = 2\pi/\lambda_{\mathrm{T}}$ is the wavevector of the optical lattice at wavelength λ_{T} and $V_{0,i}$ is the trap depth experienced by an atom in the ground ($i = g$) or the excited ($i = e$) state. The energy levels and the corresponding wavefunctions of a particle moving in a potential as in eq. (5.13) are the solutions of a Mathieu equation [223]. These are computed using Wolfram Mathematica separately before starting the simulation in Python.

The initial bound levels populations are calculated by assuming that Li atoms are suddenly transferred from a free particle state to a bound level state. The atoms are initially assumed to be well described by a Gaussian wavepacket

$$\psi_\sigma(x) = \frac{1}{\sqrt{\sigma\sqrt{2\pi}}}\, e^{-\frac{x^2}{4\sigma^2}}\, e^{i\frac{p_0}{\hbar}x}\,,$$

where σ is the spatial extension of the wavepacket at $t = 0$, $p_0 = \sqrt{mk_BT_0}$ is the momentum associated with the group velocity of the wavepacket and k_B is the Boltzmann constant. The population of the n-th bound level is $\Pi_n = c_n^2$, where:

$$c_n = \frac{1}{\sqrt{\sigma\sqrt{2\pi}}}\,\frac{1}{\sqrt{2^n n!\sqrt{\pi}}}\left(\frac{m\omega_T}{\hbar}\right)^{1/4}\int_{-\infty}^{\infty} e^{-\left(\frac{m\omega_T}{2\hbar}+\frac{1}{4\sigma^2}\right)x^2 + i\frac{p_0}{\hbar}x}\, H_n\!\left(\sqrt{\frac{m\omega_T}{\hbar}}\,x\right).$$

By substituting the Hermite polynomials $H_n(x)$ with the Gould-Hopper polynomials[3] $H_n(x, y)$ using the relation $H_n(2x, -1) = H_n(x)$, the integral can be rewritten in a solvable form [224]. The initial temperature and dimension of the atomic cloud are chosen to be $T_0 = 40\,\mu\text{K}$ and $\sigma = 500\,\mu\text{m}$ since these values are commonly observed in experiments involving lithium [126]. With these conditions the initial average occupation number is calculated to be 16.2.

The hyperfine levels are initialized with equal population, *i.e.* the atomic cloud is not in a polarized state. Throughout the simulation the magnetic field is assumed constant and at a low value (near 0 G), this choice also makes it possible to neglect the atom-atom collision interactions which tend to play a role near high-field Feshbach resonances.

Results of the numeric solution of eq. (5.10) are shown in fig. 5.7. The final occupation number (averaged over different hyperfine levels) is 0.7, with a corresponding ground state occupation probability of 47.7 %.

Due to the hyperfine configuration of Li the system can be efficiently cooled by using three laser frequencies (the addressed transitions are shown in the inset of fig. 5.7) swept together. The light detunings with respect to the fine structure D_1 transition of Lithium are set to: Δ_0 from $-67.35\,\text{MHz}$ to $-12.65\,\text{MHz}$, Δ_1 from $-93.45\,\text{MHz}$ to $-38.75\,\text{MHz}$ and Δ_2 from $160.8\,\text{MHz}$ to $215.5\,\text{MHz}$.

The bound levels' energies (and thus the sideband transitions) are also dependent on the radial position of the atom in the optical trapping potential. Generally, in an atomic cloud confined in an optical lattice the atoms do not lay exactly on the trap axis where the potential depth is maximal. In order to estimate the effects of the radial distribution of a particle within a single lattice site, the simulation is run multiple times with the atom displaced at a distance x from the trap axis.

[3] These are the solutions to the heat Fourier equation and are different from the usual definition of bivariate Hermite polynomials.

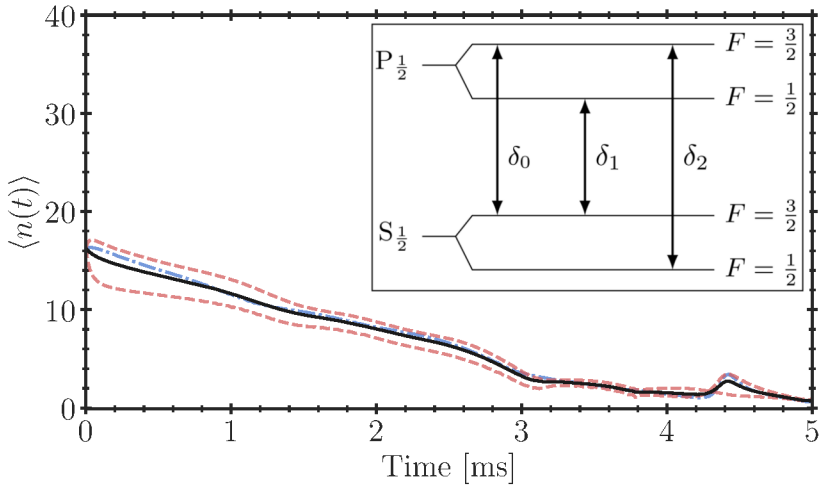

Figure 5.7: Average occupation number of Li atoms in the $F = 3/2$ (red dashed lined) and $F = 1/2$ (blue dotted line) states as a function of time. The black solid line shows the average of the hyperfine levels. Inset: internal levels of the electronic ground state of ^{6}Li. The arrows indicate the transitions that were addressed in the simulation.

Since a standing wave trap is considerably shallower along the transversal axis, x can be approximated as a classical variable. Figure 5.8 shows the results of these simulations, the cooling laser sweep parameters are left as previously indicated.

Due to the different bound state configuration, the laser sweep can only cool efficiently the atoms located near the trap axis while atoms located at a distance greater than $\geq 10\,\%$ of the trap waist will experience heating. Assuming that the radial density of the atomic cloud follows a Boltzmann distribution, for an initial temperature of $T = 40\,\mu\text{K}$ the width of the radial density distribution is approximately $10\,\mu\text{m}$, i.e. $8.6\,\%$ of the optical lattice waist.

Given these sweep detunings, at higher magnetic fields we observe that cooling is no longer efficient for some hyperfine states, in particular when the magnetic field is increased over $20\,\text{G}$ several hyperfine states become weakly resonant with the cooling laser and, therefore, are not cooled effectively.

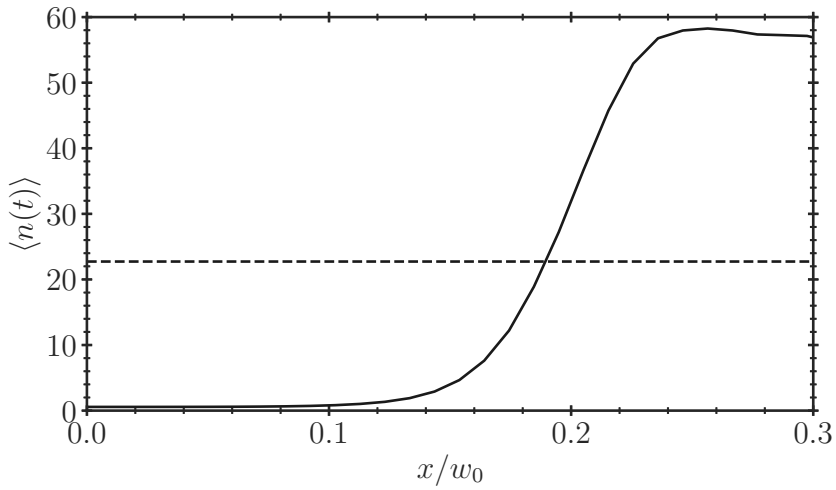

Figure 5.8: Final average occupation number as a function of the atoms' position along the trap radial axis x. Dashed line indicates the initial average occupation number. The x-axis is in units of the trap laser waist w_0.

Bibliography

[1] L. Fallani and A. Kastberg. "Cold atoms: A field enabled by light". In: *EPL (Europhysics Letters)* 110.5 (June 2015), p. 53001. DOI: 10.1209/0295-5075/110/53001.

[2] Cheng Chin et al. "Feshbach resonances in ultracold gases". In: *Reviews of Modern Physics* 82.2 (Apr. 2010), pp. 1225–1286. DOI: 10.1103/revmodphys.82.1225.

[3] M. Saffman, T. G. Walker, and K. Mølmer. "Quantum information with Rydberg atoms". In: *Reviews of Modern Physics* 82.3 (Aug. 2010), pp. 2313–2363. DOI: 10.1103/revmodphys.82.2313.

[4] Maciej Lewenstein et al. "Ultracold atomic gases in optical lattices: mimicking condensed matter physics and beyond". In: *Advances in Physics* 56.2 (Mar. 2007), pp. 243–379. DOI: 10.1080/00018730701223200.

[5] Omjyoti Dutta et al. "Non-standard Hubbard models in optical lattices: a review". In: *Reports on Progress in Physics* 78.6 (May 2015), p. 066001. DOI: 10.1088/0034-4885/78/6/066001.

[6] F. Nogrette et al. "Single-Atom Trapping in Holographic 2D Arrays of Microtraps with Arbitrary Geometries". In: *Physical Review X* 4.2 (May 2014), p. 021034. DOI: 10.1103/physrevx.4.021034.

[7] I. Bloch. "Quantum Gases". In: *Science* 319.5867 (Feb. 2008), pp. 1202–1203. DOI: 10.1126/science.1152501.

[8] R Miller et al. "Trapped atoms in cavity QED: coupling quantized light and matter". In: *Journal of Physics B: Atomic, Molecular and Optical Physics* 38.9 (Apr. 2005), S551–S565. DOI: 10.1088/0953-4075/38/9/007.

[9] Immanuel Bloch, Jean Dalibard, and Wilhelm Zwerger. "Many-body physics with ultracold gases". In: *Reviews of Modern Physics* 80.3 (July 2008), pp. 885–964. DOI: 10.1103/revmodphys.80.885.

[10] Stefano Giorgini, Lev P. Pitaevskii, and Sandro Stringari. "Theory of ultracold atomic Fermi gases". In: *Reviews of Modern Physics* 80.4 (Oct. 2008), pp. 1215–1274. DOI: 10.1103/revmodphys.80.1215.

[11] Immanuel Bloch, Jean Dalibard, and Sylvain Nascimbène. "Quantum simulations with ultracold quantum gases". In: *Nature Physics* 8.4 (Apr. 2012), pp. 267–276. DOI: 10.1038/nphys2259.

[12] Hannes Bernien et al. "Probing many-body dynamics on a 51-atom quantum simulator". In: *Nature* 551.7682 (Nov. 2017), pp. 579–584. DOI: 10.1038/nature24622.

[13] D. Jaksch and P. Zoller. "The cold atom Hubbard toolbox". In: *Annals of Physics* 315.1 (Jan. 2005), pp. 52–79. DOI: 10.1016/j.aop.2004.09.010.

[14] C. Monroe. "Quantum information processing with atoms and photons". In: *Nature* 416.6877 (Mar. 2002), pp. 238–246. DOI: 10.1038/416238a.

[15] Th. Udem, R. Holzwarth, and T. W. Hänsch. "Optical frequency metrology". In: *Nature* 416.6877 (Mar. 2002), pp. 233–237. DOI: 10.1038/416233a.

[16] Susannah M. Dickerson et al. "Multiaxis Inertial Sensing with Long-Time Point Source Atom Interferometry". In: *Physical Review Letters* 111.8 (Aug. 2013), p. 083001. DOI: 10.1103/physrevlett.111.083001.

[17] Brenton C. Young et al. "Lasers for an optical frequency standard using trapped Hg^+ ions". In: AIP, 1999. DOI: 10.1063/1.57474.

[18] Ch. Roos et al. "Quantum State Engineering on an Optical Transition and Decoherence in a Paul Trap, Ion". In: *Physical Review Letters* 83.23 (Dec. 1999), pp. 4713–4716. DOI: 10.1103/physrevlett.83.4713.

[19] Pengfei Wang et al. "Single ion qubit with estimated coherence time exceeding one hour". In: *Nature Communications* 12.1 (Jan. 2021). DOI: 10.1038/s41467-020-20330-w.

[20] N. Huntemann et al. "Single-Ion Atomic Clock with 3×10^{-18} Systematic Uncertainty". In: *Physical Review Letters* 116.6 (Feb. 2016), p. 063001. DOI: 10.1103/physrevlett.116.063001.

[21] F DiFilippo et al. "Accurate atomic mass measurements from Penning trap mass comparisons of individual ions". In: *Physica Scripta* T59 (Jan. 1995), pp. 144–154. DOI: 10.1088/0031-8949/1995/t59/018.

[22] Michael Drewsen. "Ion Coulomb crystals". In: *Physica B: Condensed Matter* 460 (Mar. 2015), pp. 105–113. DOI: 10.1016/j.physb.2014.11.050.

[23] R. Blümel et al. "Chaos and order of laser-cooled ions in a Paul trap". In: *Physical Review A* 40.2 (July 1989), pp. 808–823. DOI: 10.1103/physreva.40.808.

[24] H. M. VAN HORN. "Dense Astrophysical Plasmas". In: *Science* 252.5004 (Apr. 1991), pp. 384–389. DOI: 10.1126/science.252.5004.384.

[25] Peter Horak, Aurélien Dantan, and Michael Drewsen. "Optically induced structural phase transitions in ion Coulomb crystals". In: *Physical Review A* 86.4 (Oct. 2012), p. 043435. DOI: 10.1103/physreva.86.043435.

[26] Klaus Mølmer and Anders Sørensen. "Multiparticle Entanglement of Hot Trapped Ions". In: *Physical Review Letters* 82.9 (Mar. 1999), pp. 1835–1838. DOI: 10.1103/physrevlett.82.1835.

[27] I. Pogorelov et al. "Compact Ion-Trap Quantum Computing Demonstrator". In: *PRX Quantum* 2.2 (June 2021), p. 020343. DOI: 10.1103/prxquantum.2.020343.

[28] Michał Tomza et al. "Cold hybrid ion-atom systems". In: *Rev. Mod. Phys. 91, 035001 (2019)* (Aug. 2017). DOI: 10.1103/RevModPhys.91.035001. arXiv: 1708.07832 [physics.atom-ph].

[29] Zbigniew Idziaszek et al. "Multichannel quantum-defect theory for ultracold atom-ion collisions". In: *New Journal of Physics* 13.8 (Aug. 2011), p. 083005. DOI: 10.1088/1367-2630/13/8/083005.

[30] Pascal Weckesser et al. "Observation of Feshbach resonances between a single ion and ultracold atoms". In: (May 2021). arXiv: 2105.09382 [physics.atom-ph].

[31] Felix H. J. Hall et al. "Light-Assisted Ion-Neutral Reactive Processes in the Cold Regime: Radiative Molecule Formation versus Charge Exchange". In: *Physical Review Letters* 107.24 (Dec. 2011), p. 243202. DOI: 10.1103/physrevlett.107.243202.

[32] Arne Härter et al. "Single Ion as a Three-Body Reaction Center in an Ultracold Atomic Gas". In: *Physical Review Letters* 109.12 (Sept. 2012), p. 123201. DOI: 10.1103/physrevlett.109.123201.

[33] Tomas Sikorsky et al. "Spin-controlled atom-ion chemistry". In: *Nature Communications* 9.1 (Mar. 2018). DOI: 10.1038/s41467-018-03373-y.

[34] Lothar Ratschbacher et al. "Controlling chemical reactions of a single particle". In: *Nature Physics* 8.9 (July 2012), pp. 649–652. DOI: 10.1038/nphys2373.

[35] Theodore P. Snow and Veronica M. Bierbaum. "Ion Chemistry in the Interstellar Medium". In: *Annual Review of Analytical Chemistry* 1.1 (July 2008), pp. 229–259. DOI: 10.1146/annurev.anchem.1.031207.112907.

[36] U. Bissbort et al. "Emulating Solid-State Physics with a Hybrid System of Ultracold Ions and Atoms". In: *Physical Review Letters* 111.8 (Aug. 2013), p. 080501. DOI: 10.1103/physrevlett.111.080501.

[37] Michael Knap et al. "Time-Dependent Impurity in Ultracold Fermions: Orthogonality Catastrophe and Beyond". In: *Physical Review X* 2.4 (Dec. 2012), p. 041020. DOI: 10.1103/physrevx.2.041020.

[38] D. J. Larson et al. "Sympathetic cooling of trapped ions: A laser-cooled two-species nonneutral ion plasma". In: *Physical Review Letters* 57.1 (July 1986), pp. 70–73. DOI: 10.1103/physrevlett.57.70.

[39] A. Kellerbauer et al. "Buffer gas cooling of ion beams". In: *Nuclear Instruments and Methods in Physics Research Section A: Accelerators, Spectrometers, Detectors and Associated Equipment* 469.2 (Aug. 2001), pp. 276–285. DOI: 10.1016/s0168-9002(01)00286-8.

[40] Corinna Kollath, Michael Köhl, and Thierry Giamarchi. "Scanning tunneling microscopy for ultracold atoms". In: *Physical Review A* 76.6 (Dec. 2007), p. 063602. DOI: 10.1103/physreva.76.063602.

[41] Andrew T. Grier et al. "Observation of Cold Collisions between Trapped Ions and Trapped Atoms". In: *Physical Review Letters* 102.22 (June 2009), p. 223201. DOI: 10.1103/physrevlett.102.223201.

[42] Oleg P. Makarov et al. "Radiative charge-transfer lifetime of the excited state of $(NaCa^+)$". In: *Physical Review A* 67.4 (Apr. 2003), p. 042705. DOI: 10.1103/physreva.67.042705.

[43] Ziv Meir et al. "Experimental apparatus for overlapping a ground-state cooled ion with ultracold atoms". In: *Journal of Modern Optics* 65.5-6 (Nov. 2017), pp. 501–519. DOI: 10.1080/09500340.2017.1397217.

[44] Shinsuke Haze et al. "Observation of elastic collisions between lithium atoms and calcium ions". In: *Physical Review A* 87.5 (May 2013), p. 052715. DOI: 10.1103/physreva.87.052715.

[45] Winthrop W. Smith, Oleg P. Makarov, and Jian Lin. "Cold ion-neutral collisions in a hybrid trap". In: *Journal of Modern Optics* 52.16 (Nov. 2005), pp. 2253–2260. DOI: 10.1080/09500340500275850.

[46] Christoph Zipkes et al. "A trapped single ion inside a Bose-Einstein condensate". In: *Nature* 464.7287 (Mar. 2010), pp. 388–391. DOI: 10.1038/nature08865.

[47] L. Ratschbacher et al. "Decoherence of a Single-Ion Qubit Immersed in a Spin-Polarized Atomic Bath". In: *Physical Review Letters* 110.16 (Apr. 2013), p. 160402. DOI: 10.1103/physrevlett.110.160402.

[48] Stefan Schmid, Arne Härter, and Johannes Hecker Denschlag. "Dynamics of a Cold Trapped Ion in a Bose-Einstein Condensate". In: *Physical Review Letters* 105.13 (Sept. 2010), p. 133202. DOI: 10.1103/physrevlett.105.133202.

[49] A. Härter and J. Hecker Denschlag. "Cold atom-ion experiments in hybrid traps". In: *Contemporary Physics* 55.1 (Jan. 2014), pp. 33–45. DOI: 10.1080/00107514.2013.854618.

[50] Carlo Sias and Michael Köhl. "Hybrid quantum systems of ions and atoms". In: (Jan. 2014). arXiv: 1401.3188 [cond-mat.quant-gas].

[51] Ch. Schneider et al. "Optical trapping of an ion". In: *Nature Photonics* 4.11 (Oct. 2010), pp. 772–775. DOI: 10.1038/nphoton.2010.236.

[52] Thomas Huber et al. "A far-off-resonance optical trap for a Ba+ ion". In: *Nat Commun* 5 (2014), p. 5587. ISSN: 2041-1723. DOI: 10.1038/ncomms6587.

[53] Elia Perego, Lucia Duca, and Carlo Sias. "Electro-Optical Ion Trap for Experiments with Atom-Ion Quantum Hybrid Systems". In: *Applied Sciences* 10.7 (Mar. 2020), p. 2222. DOI: 10.3390/app10072222.

[54] T. Schmid et al. "Rydberg Molecules for Ion-Atom Scattering in the Ultracold Regime". In: *Physical Review Letters* 120.15 (Apr. 2018), p. 153401. DOI: 10.1103/physrevlett.120.153401.

[55] Philipp Wessels et al. "Absolute strong-field ionization probabilities of ultracold rubidium atoms". In: *Communications Physics* 1.1 (July 2018). DOI: 10.1038/s42005-018-0032-5.

[56] Christoph Zipkes. "A Trapped Single Ion Inside a Bose-Einstein Condensate". PhD thesis. Robinson College, Cambridge, 2011.

[57] Marko Cetina, Andrew T. Grier, and Vladan Vuletić. "Micromotion-Induced Limit to Atom-Ion Sympathetic Cooling in Paul Traps". In: 109.25 (Dec. 2012), p. 253201. DOI: 10.1103/physrevlett.109.253201.

[58] Christoph Zipkes et al. "Kinetics of a single trapped ion in an ultracold buffer gas". In: 13.5 (May 2011), p. 053020. DOI: 10.1088/1367-2630/13/5/053020.

[59] P Langevin. "Une formule fondamentale de théorie cinétique". In: *Ann. Chim. et Physique* 5 (1905), pp. 269–300.

[60] Leonard Schiff. *Quantum mechanics*. 3rd edition. New York: McGraw-Hill, 1968. ISBN: 978-0070856431.

[61] E. Tiesinga et al. "A spectroscopic determination of scattering lengths for sodium atom collisions". In: *Journal of Research of the National Institute of Standards and Technology* 101.4 (July 1996), p. 505. DOI: 10.6028/jres.101.051.

[62] R. Côté and A. Dalgarno. "Ultracold atom-ion collisions". In: *Physical Review A* 62.1 (June 2000), p. 012709. DOI: 10.1103/physreva.62.012709.

[63] J Hasted. "Inelastic collisions between ions and atoms". In: *Proc. R. Soc. Lond. A*. Vol. 212. 1952, pp. 235–248. DOI: 10.1098/rspa.1952.0078.

[64] H. Schmaljohann et al. "Dynamics and thermodynamics in spinor quantum gases". In: *Applied Physics B* 79.8 (Dec. 2004), pp. 1001–1007. DOI: 10.1007/s00340-004-1664-6.

[65] David Reens et al. “Controlling spin flips of molecules in an electromagnetic trap”. In: *Physical Review A* 96.6 (Dec. 2017), p. 063420. DOI: 10.1103/physreva.96.063420.

[66] Giacomo Cappellini. “Two-orbital quantum phyics in Yb Fermi gases expliting the $^1S_0 \rightarrow {}^3P_0$ clock transition”. PhD thesis. University of Florence, 2015.

[67] Moritz Höfer. “A two-orbital quantum gas with tunable interactions”. PhD thesis. University of Munich, 2017.

[68] Marco Anderlini et al. “Controlled exchange interaction between pairs of neutral atoms in an optical lattice”. In: *Nature* 448.7152 (July 2007), pp. 452–456. DOI: 10.1038/nature06011.

[69] Wade G. Rellergert et al. “Measurement of a Large Chemical Reaction Rate between Ultracold Closed-Shell ^{40}Ca Atoms and Open-Shell $^{174}Yb^+$ Ions Held in a Hybrid Atom-Ion Trap”. In: *Physical Review Letters* 107.24 (Dec. 2011), p. 243201. DOI: 10.1103/physrevlett.107.243201.

[70] Felix H.J. Hall et al. “Ion-neutral chemistry at ultralow energies: dynamics of reactive collisions between laser-cooled Ca^+ ions and Rb atoms in an ion-atom hybrid trap”. In: *Molecular Physics* 111.14-15 (Apr. 2013), pp. 2020–2032. DOI: 10.1080/00268976.2013.780107.

[71] Felix H. J. Hall and Stefan Willitsch. “Millikelvin Reactive Collisions between Sympathetically Cooled Molecular Ions and Laser-Cooled Atoms in an Ion-Atom Hybrid Trap”. In: *Physical Review Letters* 109.23 (Dec. 2012), p. 233202. DOI: 10.1103/physrevlett.109.233202.

[72] Christoph Zipkes et al. “Cold Heteronuclear Atom-Ion Collisions”. In: *Physical Review Letters* 105.13 (Sept. 2010), p. 133201. DOI: 10.1103/physrevlett.105.133201.

[73] Artjom Krükow et al. “Reactive two-body and three-body collisions of Ba^+ in an ultracold Rb gas”. In: *Physical Review A* 94.3 (Sept. 2016), p. 030701. DOI: 10.1103/physreva.94.030701.

[74] Artjom Krükow. “Three-Body Reaction Dynamics in cold Atom-Ion Experiments”. PhD thesis. Universität Ulm, 2016.

[75] Jesús Pérez-Ríos. “Vibrational quenching and reactive processes of weakly bound molecular ions colliding with atoms at cold temperatures”. In: *Physical Review A* 99.2 (Feb. 2019), p. 022707. DOI: 10.1103/physreva.99.022707.

[76] M. Knoop, M. Vedel, and F. Vedel. “Lifetime, collisional-quenching, and j-mixing measurements of the metastable 3Dlevels of Ca^+”. In: *Physical Review A* 52.5 (Nov. 1995), pp. 3763–3769. DOI: 10.1103/physreva.52.3763.

[77] J. Deiglmayr et al. "Reactive collisions of trapped anions with ultracold atoms". In: *Physical Review A* 86.4 (Oct. 2012), p. 043438. DOI: 10.1103/physreva.86.043438.

[78] Stefan Willitsch et al. "Cold Reactive Collisions between Laser-Cooled Ions and Velocity-Selected Neutral Molecules". In: *Physical Review Letters* 100.4 (Jan. 2008), p. 043203. DOI: 10.1103/physrevlett.100.043203.

[79] B. Roth et al. "Ion-neutral chemical reactions between ultracold localized ions and neutral molecules with single-particle resolution". In: *Physical Review A* 73.4 (Apr. 2006), p. 042712. DOI: 10.1103/physreva.73.042712.

[80] Peter F. Staanum et al. "Probing Isotope Effects in Chemical Reactions Using Single Ions". In: *Physical Review Letters* 100.24 (June 2008), p. 243003. DOI: 10.1103/physrevlett.100.243003.

[81] Dieter Gerlich and Stevan Horning. "Experimental investigation of radiative association processes as related to interstellar chemistry". In: *Chemical Reviews* 92.7 (Nov. 1992), pp. 1509–1539. DOI: 10.1021/cr00015a003.

[82] Hauke Doerk, Zbigniew Idziaszek, and Tommaso Calarco. "Atom-ion quantum gate". In: *Physical Review A* 81.1 (Jan. 2010), p. 012708. DOI: 10.1103/physreva.81.012708.

[83] Lê Huy Nguyên et al. "Micromotion in trapped atom-ion systems". In: *Physical Review A* 85.5 (May 2012), p. 052718. DOI: 10.1103/physreva.85.052718.

[84] T. Secker et al. "Controlled long-range interactions between Rydberg atoms and ions". In: *Physical Review A* 94.1 (July 2016), p. 013420. DOI: 10.1103/physreva.94.013420.

[85] Anders Sørensen and Klaus Mølmer. "Quantum Computation with Ions in Thermal Motion". In: *Physical Review Letters* 82.9 (Mar. 1999), pp. 1971–1974. DOI: 10.1103/physrevlett.82.1971.

[86] Richard P. Feynman. "Simulating physics with computers". In: *International Journal of Theoretical Physics* 21.6-7 (June 1982), pp. 467–488. DOI: 10.1007/bf02650179.

[87] R. Blatt and C. F. Roos. "Quantum simulations with trapped ions". In: *Nature Physics* 8.4 (Apr. 2012), pp. 277–284. DOI: 10.1038/nphys2252.

[88] A. Negretti et al. "Generalized Kronig-Penney model for ultracold atomic quantum systems". In: *Physical Review B* 90.15 (Oct. 2014), p. 155426. DOI: 10.1103/physrevb.90.155426.

[89] Christoph Maschler and Helmut Ritsch. "Cold Atom Dynamics in a Quantum Optical Lattice Potential". In: *Physical Review Letters* 95.26 (Dec. 2005), p. 260401. DOI: 10.1103/physrevlett.95.260401.

[90] R. Gerritsma et al. "Bosonic Josephson Junction Controlled by a Single Trapped Ion". In: *Physical Review Letters* 109.8 (Aug. 2012), p. 080402. DOI: 10.1103/physrevlett.109.080402.

[91] Daniel Keefer and Regina de Vivie-Riedle. "Pathways to New Applications for Quantum Control". In: *Accounts of Chemical Research* 51.9 (Aug. 2018), pp. 2279–2286. DOI: 10.1021/acs.accounts.8b00244.

[92] Jennifer L. Herek et al. "Quantum control of energy flow in light harvesting". In: *Nature* 417.6888 (May 2002), pp. 533–535. DOI: 10.1038/417533a.

[93] A. Assion. "Control of Chemical Reactions by Feedback-Optimized Phase-Shaped Femtosecond Laser Pulses". In: *Science* 282.5390 (Oct. 1998), pp. 919–922. DOI: 10.1126/science.282.5390.919.

[94] L. Zhu et al. "Coherent Laser Control of the Product Distribution Obtained in the Photoexcitation of HI". In: *Science* 270.5233 (Oct. 1995), pp. 77–80. DOI: 10.1126/science.270.5233.77.

[95] Felix H.J. Hall et al. "Light-assisted cold chemical reactions of barium ions with rubidium atoms". In: *Molecular Physics* 111.12-13 (June 2013), pp. 1683–1690. DOI: 10.1080/00268976.2013.770930.

[96] Xin Tong et al. "State-selected ion-molecule reactions with Coulomb-crystallized molecular ions in traps". In: *Chemical Physics Letters* 547 (Sept. 2012), pp. 1–8. DOI: 10.1016/j.cplett.2012.06.042.

[97] Brianna R. Heazlewood and Timothy P. Softley. "Low-Temperature Kinetics and Dynamics with Coulomb Crystals". In: *Annual Review of Physical Chemistry* 66.1 (Apr. 2015), pp. 475–495. DOI: 10.1146/annurev-physchem-040214-121527.

[98] N. Poli et al. "Optical atomic clocks". In: *La rivista del Nuovo Cimento - Vol. 036 - Issue 12 - Pag. 555-624 - Year 2013* 36 (Jan. 2014), pp. 555–624. ISSN: 0393697X, 0393697X. DOI: 10.1393/ncr/i2013-10095-x. arXiv: 1401.2378 [physics.atom-ph].

[99] Andrew D. Ludlow et al. "Optical atomic clocks". In: *Reviews of Modern Physics* 87.2 (June 2015), pp. 637–701. DOI: 10.1103/revmodphys.87.637.

[100] Gretchen K Campbell et al. "The absolute frequency of the ^{87}Sr optical clock transition". In: *Metrologia* 45.5 (Sept. 2008), pp. 539–548. DOI: 10.1088/0026-1394/45/5/008.

[101] C. Champenois et al. "Ion ring in a linear multipole trap for optical frequency metrology". In: *Physical Review A* 81.4 (Apr. 2010), p. 043410. DOI: 10.1103/physreva.81.043410.

[102] Tobias Bothwell et al. "JILA SrI optical lattice clock with uncertainty of 2.0×10^{-18}". In: *Metrologia* 56.6 (Oct. 2019), p. 065004. DOI: 10.1088/1681-7575/ab4089.

[103] W. F. McGrew et al. "Atomic clock performance enabling geodesy below the centimetre level". In: *Nature* 564.7734 (Nov. 2018), pp. 87–90. DOI: 10.1038/s41586-018-0738-2.

[104] Amar C. Vutha, Tom Kirchner, and Pierre Dubé. "Collisional frequency shift of a trapped-ion optical clock". In: *Physical Review A* 96.2 (Aug. 2017), p. 022704. DOI: 10.1103/physreva.96.022704.

[105] A. M. Hankin et al. "Systematic uncertainty due to background-gas collisions in trapped-ion optical clocks". In: *Physical Review A* 100.3 (Sept. 2019), p. 033419. DOI: 10.1103/physreva.100.033419.

[106] T. Rosenband et al. "Observation of the $^1S_0 \rightarrow {}^2P_0$ Clock Transition $^{27}Al^+$". In: *Physical Review Letters* 98.22 (May 2007), p. 220801. DOI: 10.1103/physrevlett.98.220801.

[107] Eric R. Hudson. "Sympathetic cooling of molecular ions with ultracold atoms". In: *EPJ Techniques and Instrumentation* 3.1 (Dec. 2016). DOI: 10.1140/epjti/s40485-016-0035-0.

[108] Peter Van Der Straten H. J. Metcalf. *Laser Cooling and Trapping*. SPRINGER NATURE, Sept. 1999. 323 pp. ISBN: 0387987479.

[109] D.A. Steck. *Quantum and Atom Optics*. URL: http://steck.us/teaching.

[110] Keith D. Bonin Vitaly V Kresin. *Electric-Dipole Polarizabilities of Atoms, Molecules, and Clusters*. WSPC, Nov. 1997. 270 pp. ISBN: 9810224931.

[111] John V. Prodan and William D. Phillips. "Chirping the light—fantastic? Recent NBS atom cooling experiments". In: 8.3-4 (Jan. 1984), pp. 231–235. DOI: 10.1016/0079-6727(84)90019-3.

[112] John V. Prodan, William D. Phillips, and Harold Metcalf. "Laser Production of a Very Slow Monoenergetic Atomic Beam". In: 49.16 (Oct. 1982), pp. 1149–1153. DOI: 10.1103/physrevlett.49.1149.

[113] T.W. Hänsch and A.L. Schawlow. "Cooling of gases by laser radiation". In: 13.1 (Jan. 1975), pp. 68–69. DOI: 10.1016/0030-4018(75)90159-5.

[114] K. Kowalski et al. "Magneto-optical Trap: Fundamentals and Realization". In: (2010). DOI: 10.12921/CMST.2010.SI.02.115-129.

[115] Christopher J. Foot. *Atomic Physics*. OXFORD UNIV PR, Jan. 2005. 346 pp. ISBN: 0198506961.

[116] Wolfgang Petrich et al. "Behavior of atoms in a compressed magneto-optical trap". In: 11.8 (Aug. 1994), p. 1332. DOI: 10.1364/josab.11.001332.

[117] M. Drewsen et al. “Investigation of sub-Doppler cooling effects in a cesium magneto-optical trap”. In: 59.3 (Sept. 1994), pp. 283–298. DOI: 10.1007/bf01081396.

[118] Giacomo Valtolina. “Development of an experimental apparatus for the production and study of ultracold atomic gases of fermionic lithium”. MA thesis. Università degli studi di Milano, 2012.

[119] Paul D. Lett et al. “Observation of Atoms Laser Cooled below the Doppler Limit”. In: 61.2 (July 1988), pp. 169–172. DOI: 10.1103/physrevlett.61.169.

[120] J. Dalibard and C. Cohen-Tannoudji. “Laser cooling below the Doppler limit by polarization gradients: simple theoretical models”. In: 6.11 (Nov. 1989), p. 2023. DOI: 10.1364/josab.6.002023.

[121] Claude N. Cohen-Tannoudji and William D. Phillips. “New Mechanisms for Laser Cooling”. In: 43.10 (Oct. 1990), pp. 33–40. DOI: 10.1063/1.881239.

[122] A. Aspect et al. “Laser Cooling below the One-Photon Recoil Energy by Velocity-Selective Coherent Population Trapping”. In: *Physical Review Letters* 61.7 (Aug. 1988), pp. 826–829. DOI: 10.1103/physrevlett.61.826.

[123] M. S. Shahriar et al. “Continuous polarization-gradient precooling-assisted velocity-selective coherent population trapping”. In: 48.6 (Dec. 1993), R4035–R4038. DOI: 10.1103/physreva.48.r4035.

[124] M Weidemüller et al. “A Novel Scheme for Efficient Cooling below the Photon Recoil Limit”. In: 27.2 (July 1994), pp. 109–114. DOI: 10.1209/0295-5075/27/2/006.

[125] M A Ol-shanii and V G Minogin. “Three-dimensional velocity-selective coherent population trapping of (3+1)-level atoms”. In: 3.6 (Dec. 1991), pp. 317–322. DOI: 10.1088/0954-8998/3/6/001.

[126] A. Burchianti et al. “Efficient all-optical production of largeLi6quantum gases usingD1gray-molasses cooling”. In: *Physical Review A* 90.4 (Oct. 2014), p. 043408. DOI: 10.1103/physreva.90.043408.

[127] Paul Hamilton et al. “Sisyphus cooling of lithium”. In: 89.2 (Feb. 2014), p. 023409. DOI: 10.1103/physreva.89.023409.

[128] Gregers Poulsen. “Sideband Cooling of Atomic and Molecular Ions”. PhD thesis. University of Aarhus, 2011.

[129] Stig Stenholm. “The semiclassical theory of laser cooling”. In: 58.3 (July 1986), pp. 699–739. DOI: 10.1103/revmodphys.58.699.

[130] Immanuel Bloch. “Ultracold quantum gases in optical lattices”. In: *Nature Physics* 1.1 (Oct. 2005), pp. 23–30. DOI: 10.1038/nphys138.

[131] Cecilia Muldoon et al. “Control and manipulation of cold atoms in optical tweezers”. In: *New Journal of Physics* 14.7 (July 2012), p. 073051. DOI: 10.1088/1367-2630/14/7/073051.

[132] C. Ospelkaus et al. “Ultracold Heteronuclear Molecules in a 3D Optical Lattice”. In: *Physical Review Letters* 97.12 (Sept. 2006), p. 120402. DOI: 10.1103/physrevlett.97.120402.

[133] Loïc Anderegg et al. “An optical tweezer array of ultracold molecules”. In: *Science* 365.6458 (Sept. 2019), pp. 1156–1158. DOI: 10.1126/science.aax1265.

[134] David G. Grier and Yael Roichman. “Holographic optical trapping”. In: 45.5 (Feb. 2006), p. 880. DOI: 10.1364/ao.45.000880.

[135] A. Mosk et al. “Resonator-enhanced optical dipole trap for fermionic lithium atoms”. In: *Optics Letters* 26.23 (Dec. 2001), p. 1837. DOI: 10.1364/ol.26.001837.

[136] Nicolas Schlosser et al. “Sub-poissonian loading of single atoms in a microscopic dipole trap”. In: *Nature* 411.6841 (June 2001), pp. 1024–1027. DOI: 10.1038/35082512.

[137] Mark Kasevich and Steven Chu. “Laser cooling below a photon recoil with three-level atoms”. In: 69.12 (Sept. 1992), pp. 1741–1744. DOI: 10.1103/physrevlett.69.1741.

[138] Simon Stellmer et al. “Laser Cooling to Quantum Degeneracy”. In: 110.26 (June 2013), p. 263003. DOI: 10.1103/physrevlett.110.263003.

[139] Jiazhong Hu et al. “Creation of a Bose-condensed gas of87Rb by laser cooling”. In: *Science* 358.6366 (Nov. 2017), pp. 1078–1080. DOI: 10.1126/science.aan5614.

[140] Wolfgang Ketterle and N.J. Van Druten. “Evaporative Cooling of Trapped Atoms”. In: *Advances In Atomic, Molecular, and Optical Physics*. Elsevier, 1996, pp. 181–236. DOI: 10.1016/s1049-250x(08)60101-9.

[141] K. B. Davis, M. -O. Mewes, and W. Ketterle. “An analytical model for evaporative cooling of atoms”. In: 60.2-3 (1995), pp. 155–159. DOI: 10.1007/bf01135857.

[142] Klaus Blaum. “High-accuracy mass spectrometry with stored ions”. In: *Physics Reports* 425.1 (Mar. 2006), pp. 1–78. DOI: 10.1016/j.physrep.2005.10.011.

[143] Wolfgang Paul. “Electromagnetic traps for charged and neutral particles”. In: *Reviews of Modern Physics* 62.3 (July 1990), pp. 531–540. DOI: 10.1103/revmodphys.62.531.

[144] D. Leibfried et al. "Quantum dynamics of single trapped ions". In: *Reviews of Modern Physics* 75.1 (Mar. 2003), pp. 281–324. DOI: 10.1103/revmodphys.75.281.

[145] D. J. Berkeland et al. "Minimization of ion micromotion in a Paul trap". In: *Journal of Applied Physics* 83.10 (May 1998), pp. 5025–5033. DOI: 10.1063/1.367318.

[146] Timm F. Gloger et al. "Ion-trajectory analysis for micromotion minimization and the measurement of small forces". In: *Physical Review A* 92.4 (Oct. 2015), p. 043421. DOI: 10.1103/physreva.92.043421.

[147] Y. Ibaraki, U. Tanaka, and S. Urabe. "Detection of parametric resonance of trapped ions for micromotion compensation". In: *Applied Physics B* 105.2 (Mar. 2011), pp. 219–223. DOI: 10.1007/s00340-011-4463-x.

[148] A. Härter et al. "Minimization of ion micromotion using ultracold atomic probes". In: *Applied Physics Letters* 102.22 (June 2013), p. 221115. DOI: 10.1063/1.4809578.

[149] Christian Schneider et al. "Influence of static electric fields on an optical ion trap". In: *Physical Review A* 85.1 (Jan. 2012), p. 013422. DOI: 10.1103/physreva.85.013422.

[150] Martin Enderlein et al. "Single Ions Trapped in a One-Dimensional Optical Lattice". In: *Physical Review Letters* 109.23 (Dec. 2012), p. 233004. DOI: 10.1103/physrevlett.109.233004.

[151] Leon Karpa et al. "Suppression of Ion Transport due to Long-Lived Subwavelength Localization by an Optical Lattice". In: *Physical Review Letters* 111.16 (Oct. 2013), p. 163002. DOI: 10.1103/physrevlett.111.163002.

[152] Alexander Lambrecht et al. "Long lifetimes and effective isolation of ions in optical and electrostatic traps". In: *Nature Photonics* 11.11 (Oct. 2017), pp. 704–707. DOI: 10.1038/s41566-017-0030-2.

[153] Ziv Meir et al. "Dynamics of a Ground-State Cooled Ion Colliding with Ultracold Atoms". In: 117.24 (Dec. 2016), p. 243401. DOI: 10.1103/physrevlett.117.243401.

[154] Alexander Kramida and Yuri Ralchenko. *NIST Atomic Spectra Database, NIST Standard Reference Database 78*. en. 1999. DOI: 10.18434/T4W30F.

[155] Jasmeet Kaur et al. "Magic wavelengths in the alkaline-earth-metal ions". In: *Physical Review A* 92.3 (Sept. 2015), p. 031402. DOI: 10.1103/physreva.92.031402.

[156] Elia Perego. "A novel setup for trapping and cooling Barium ions for atom-ion experiments". PhD thesis. Politechnic of Turin, 2019.

[157] E. R. I. Abraham et al. "Singlets-wave scattering lengths ofLi6andLi7". In: *Physical Review A* 53.6 (June 1996), R3713–R3715. DOI: 10.1103/physreva.53.r3713.

[158] Randall G. Hulet, Jason H. V. Nguyen, and Ruwan Senaratne. "Methods for preparing quantum gases of lithium". In: *Review of Scientific Instruments* 91.1 (Jan. 2020), p. 011101. DOI: 10.1063/1.5131023.

[159] L. N. Rozanov. *Vacuum technique*. London New York: Taylor & Francis, 2002. ISBN: 041527351X.

[160] Robert Krebs. *The History and Use of Our Earth's Chemical Elements*. Greenwood, July 2006. 448 pp. ISBN: 0313334382.

[161] R C Weast; M J Astle; W H Beyer. *CRC Handbook of Chemistry and Physics*. Taylor & Francis Ltd, June 1984. 1604 pp. ISBN: 0367712601.

[162] P T Greenland, M A Lauder, and D J H Wort. "Atomic beam velocity distributions". In: *Journal of Physics D: Applied Physics* 18.7 (July 1985), pp. 1223–1232. DOI: 10.1088/0022-3727/18/7/009.

[163] Elettra Neri. "Mass imbalanced Fermi mixtures with 2- and 3-body resonantinteractions". PhD thesis. Università di Firenze, 2018.

[164] URL: http://quantumgases.lens.unifi.it/.

[165] M. E. Gehm. "Preparation of an Optically-Trapped Degenerate Fermi Gas of 6Li: Finding theRoute to Degeneracy". PhD thesis. Duke University, 2003.

[166] U. Schünemann et al. "Simple scheme for tunable frequency offset locking of two lasers". In: *Review of Scientific Instruments* 70.1 (Jan. 1999), pp. 242–243. DOI: 10.1063/1.1149573.

[167] Yusuke Hisai et al. "Evaluation of laser frequency offset locking using an electrical delay line". In: *Applied Optics* 57.20 (July 2018), p. 5628. DOI: 10.1364/ao.57.005628.

[168] Amnon Yariv. *Photonics : optical electronics in modern communications*. New York Oxford: Oxford University Press, 2007. ISBN: 9780195179460.

[169] C Mok et al. "Design and construction of an efficient electro-optic modulator for laser spectroscopy". In: *Canadian Journal of Physics* 84.9 (Sept. 2006), pp. 775–786. DOI: 10.1139/p06-074.

[170] Eric D. Black. "An introduction to Pound-Drever-Hall laser frequency stabilization". In: *American Journal of Physics* 69.1 (Jan. 2001), pp. 79–87. DOI: 10.1119/1.1286663.

[171] Amelia Detti. "A new experimental apparatus for atom-ion quantum mixtures". PhD thesis. University of Florence, 2019.

[172] Christopher Bowick. *RF Circuit Design*. Elsevier Science & Technology, Nov. 2007. 256 pp. ISBN: 0750685182.

[173] A Mansingh and A Dhar. "The AC conductivity and dielectric constant of lithium niobate single crystals". In: *Journal of Physics D: Applied Physics* 18.10 (Oct. 1985), pp. 2059–2071. DOI: 10.1088/0022-3727/18/10/016.

[174] H.A. Wheeler. "Simple Inductance Formulas for Radio Coils". In: *Proceedings of the IRE* 16.10 (Oct. 1928), pp. 1398–1400. DOI: 10.1109/jrproc.1928.221309.

[175] Seon-Jae Jeon and Dong-Wook Seo. "Coupling Coefficient Measurement Method with Simple Procedures Using a Two-Port Network Analyzer for a Multi-Coil WPT System". In: *Energies* 12.20 (Oct. 2019), p. 3950. DOI: 10.3390/en12203950.

[176] Lucia Duca. *private communication*. 2021.

[177] A Fabry C; Perot. "Theorie et applications d'une nouvelle methode de spectroscopie interferentielle". In: *Ann. Chim. Phys.* 16.7785 (1899), p. 7.

[178] Orazio Svelto. *Principles of Lasers*. Springer-Verlag GmbH, Aug. 2010. ISBN: 1441913017.

[179] Joseph Verdeyen. *Laser electronics*. Englewood Cliffs, N.J: Prentice Hall, 1995. ISBN: 9780137066667.

[180] Michael Hercher. "The Spherical Mirror Fabry-Perot Interferometer". In: *Applied Optics* 7.5 (May 1968), p. 951. DOI: 10.1364/ao.7.000951.

[181] G. Rempe et al. "Measurement of ultralow losses in an optical interferometer". In: *Optics Letters* 17.5 (Mar. 1992), p. 363. DOI: 10.1364/ol.17.000363.

[182] Christina J. Hood, H. J. Kimble, and Jun Ye. "Characterization of high-finesse mirrors: Loss, phase shifts, and mode structure in an optical cavity". In: *Physical Review A* 64.3 (Aug. 2001), p. 033804. DOI: 10.1103/physreva.64.033804.

[183] Dana Z. Anderson. "Alignment of resonant optical cavities". In: *Applied Optics* 23.17 (Sept. 1984), p. 2944. DOI: 10.1364/ao.23.002944.

[184] W. Koechner. "Thermal Lensing in a Nd:YAG Laser Rod". In: *Applied Optics* 9.11 (Nov. 1970), p. 2548. DOI: 10.1364/ao.9.002548.

[185] Karl Johan Åström and Richard M. Murray. *Feedback Systems. An Introduction for Scientists and Engineers*. Princeton: Princeton University Press, 2010. ISBN: 9780691135762. DOI: 10.2307/j.ctvcm4gdk.

[186] John Bechhoefer. "Feedback for physicists: A tutorial essay on control". In: *Reviews of Modern Physics* 77.3 (Aug. 2005), pp. 783–836. DOI: 10.1103/revmodphys.77.783.

[187] L. Ricci et al. "A compact grating-stabilized diode laser system for atomic physics". In: *Optics Communications* 117.5-6 (June 1995), pp. 541–549. DOI: 10.1016/0030-4018(95)00146-y.

[188] T.W. Hansch and B. Couillaud. "Laser frequency stabilization by polarization spectroscopy of a reflecting reference cavity". In: *Optics Communications* 35.3 (Dec. 1980), pp. 441–444. DOI: 10.1016/0030-4018(80)90069-3.

[189] R. W. P. Drever et al. "Laser phase and frequency stabilization using an optical resonator". In: *Applied Physics B Photophysics and Laser Chemistry* 31.2 (June 1983), pp. 97–105. DOI: 10.1007/bf00702605.

[190] Gianni Di Domenico, Stéphane Schilt, and Pierre Thomann. "Simple approach to the relation between laser frequency noise and laser line shape". In: *Applied Optics* 49.25 (Aug. 2010), p. 4801. DOI: 10.1364/ao.49.004801.

[191] Richard W. Fox, Chris W. Oates, and Leo W. Hollberg. "Stabilizing diode lasers to high-finesse cavities". In: *Cavity-Enhanced Spectroscopies*. Elsevier, 2003, pp. 1–46. DOI: 10.1016/s1079-4042(03)80017-6.

[192] Simone Borri et al. "Frequency-Noise Dynamics of Mid-Infrared Quantum Cascade Lasers". In: *IEEE Journal of Quantum Electronics* 47.7 (July 2011), pp. 984–988. DOI: 10.1109/jqe.2011.2147760.

[193] F. Berto et al. "Prospects for single-photon sideband cooling of optically trapped neutral atoms". In: *Physical Review Research* 3.4 (Nov. 2021), p. 043106. DOI: 10.1103/physrevresearch.3.043106.

[194] Michael Gröbner et al. "Degenerate Raman sideband cooling of K39". In: *Physical Review A* 95.3 (Mar. 2017), p. 033412. DOI: 10.1103/physreva.95.033412.

[195] R. Taïeb et al. "Cooling and localization of atoms in laser-induced potential wells". In: *Physical Review A* 49.6 (June 1994), pp. 4876–4887. DOI: 10.1103/physreva.49.4876.

[196] Alexandre Cooper et al. "Alkaline-Earth Atoms in Optical Tweezers". In: *Physical Review X* 8.4 (Dec. 2018), p. 041055. DOI: 10.1103/physrevx.8.041055.

[197] K. Rzążewski and R. W. Boyd. "Equivalence of interaction hamiltonians in the electric dipole approximation". In: *Journal of Modern Optics* 51.8 (May 2004), pp. 1137–1147. DOI: 10.1080/09500340408230412.

[198] Alexander L. Fetter and J. D. Walecka. *Quantum Theory of Many-Particle Systems*. Dover Publications Inc., May 2003. ISBN: 0486428273. DOI: 10.1002/9783527667550.ch8.

[199] K. B. Whaley and J. C. Light. "Rotating-frame transformations: A new approximation for multiphoton absorption and dissociation in laser fields". In: *Physical Review A* 29.3 (Mar. 1984), pp. 1188–1207. DOI: 10.1103/physreva.29.1188.

[200] J. Javanainen and S. Stenholm. "Laser cooling of trapped particles III: The Lamb-Dicke limit". In: *Applied Physics* 24.2 (Feb. 1981), pp. 151–162. DOI: 10.1007/bf00902273.

[201] G. Lindblad. "On the generators of quantum dynamical semigroups". In: *Communications in Mathematical Physics* 48.2 (June 1976), pp. 119–130. DOI: 10.1007/bf01608499.

[202] Andrzej Kossakowski Vittorio Gorini and E. C. G. Sudarshan. "Completely positive dynamical semigroups of N-level systems". In: *Journal of Mathematical Physics* 17.5 (1976), p. 821. DOI: 10.1063/1.522979.

[203] Heinz-Peter Breuer and Francesco Petruccione. *The Theory of Open Quantum Systems*. Oxford University Press, Feb. 2002. ISBN: 0198520638.

[204] Daniel Manzano. "A short introduction to the Lindblad master equation". In: *AIP Advances* 10.2 (Feb. 2020), p. 025106. DOI: 10.1063/1.5115323.

[205] A P Kazantsev, G I Surdutovich, and V P Yakovlev. *Mechanical Action of Light on Atoms*. WORLD SCIENTIFIC, Aug. 1990. DOI: 10.1142/0585.

[206] E Brion, L H Pedersen, and K Mølmer. "Adiabatic elimination in a lambda system". In: *Journal of Physics A: Mathematical and Theoretical* 40.5 (Jan. 2007), pp. 1033–1043. DOI: 10.1088/1751-8113/40/5/011.

[207] Florentin Reiter and Anders S. Sørensen. "Effective operator formalism for open quantum systems". In: *Physical Review A* 85.3 (Mar. 2012), p. 032111. DOI: 10.1103/physreva.85.032111.

[208] M. A. Norcia, A. W. Young, and A. M. Kaufman. "Microscopic Control and Detection of Ultracold Strontium in Optical-Tweezer Arrays". In: *Physical Review X* 8.4 (Dec. 2018), p. 041054. DOI: 10.1103/physrevx.8.041054.

[209] Jessie T. Zhang et al. "Forming a Single Molecule by Magnetoassociation in an Optical Tweezer". In: *Physical Review Letters* 124.25 (June 2020), p. 253401. DOI: 10.1103/physrevlett.124.253401.

[210] K.B. Blagoev and V.A. Komarovskii. "Lifetimes of Levels of Neutral and Singly Ionized Lanthanide Atoms". In: *Atomic Data and Nuclear Data Tables* 56.1 (Jan. 1994), pp. 1–40. DOI: 10.1006/adnd.1994.1001.

[211] F. Scazza. *private communication*. 2021.

[212] Y. Yu et al. "Motional-ground-state cooling outside the Lamb-Dicke regime". In: *Physical Review A* 97.6 (June 2018), p. 063423. DOI: 10.1103/physreva.97.063423.

[213] S. Saskin et al. "Narrow-Line Cooling and Imaging of Ytterbium Atoms in an Optical Tweezer Array". In: *Physical Review Letters* 122.14 (Apr. 2019), p. 143002. DOI: 10.1103/physrevlett.122.143002.

[214] M. S. Safronova, U. I. Safronova, and Charles W. Clark. "Magic wavelengths for optical cooling and trapping of lithium". In: *Physical Review A* 86.4 (Oct. 2012), p. 042505. DOI: 10.1103/physreva.86.042505.

[215] Rudolf Grimm, Matthias Weidemüller, and Yurii B. Ovchinnikov. "Optical Dipole Traps for Neutral Atoms". In: *Advances In Atomic, Molecular, and Optical Physics*. Elsevier, 2000, pp. 95–170. DOI: 10.1016/s1049-250x(08)60186-x.

[216] Jean Dalibard, Yvan Castin, and Klaus Mølmer. "Wave-function approach to dissipative processes in quantum optics". In: *Physical Review Letters* 68.5 (Feb. 1992), pp. 580–583. DOI: 10.1103/physrevlett.68.580.

[217] R. Dum, P. Zoller, and H. Ritsch. "Monte Carlo simulation of the atomic master equation for spontaneous emission". In: *Physical Review A* 45.7 (Apr. 1992), pp. 4879–4887. DOI: 10.1103/physreva.45.4879.

[218] Howard Carmichael. *An open systems approach to quantum optics : lectures presented at the Université Libre de Bruxelles October 28 to November 4, 1991*. Berlin, Heidelberg: Springer Berlin Heidelberg, 1993. ISBN: 9783540476207.

[219] G. C: Hegerfeldt and T.S. Wilser. "Ensemble or Individual System, Collapse or no Collapse: A Description of a Single Radiating Atom". In: *Classical and Quantum Systems*. Ed. by World Scientific. Proceedings of the Second International Wigner Symposium. World Scientific. 1992, pp. 104–105.

[220] J.R. Johansson, P.D. Nation, and Franco Nori. "QuTiP 2: A Python framework for the dynamics of open quantum systems". In: *Computer Physics Communications* 184.4 (Apr. 2013), pp. 1234–1240. DOI: 10.1016/j.cpc.2012.11.019.

[221] William H. Press et al. *Numerical recipes: the art of scientific computing*. Cambridge Cambridgeshire New York: Cambridge University Press, Sept. 2007. 1248 pp. ISBN: 978-0521880688.

[222] E. Wigner. "On the Quantum Correction For Thermodynamic Equilibrium". In: *Physical Review* 40.5 (June 1932), pp. 749–759. DOI: 10.1103/physrev.40.749.

[223] J. N. L. Connor et al. "Eigenvalues of the Schrödinger equation for a periodic potential with nonperiodic boundary conditions: A uniform semiclassical analysis". In: *The Journal of Chemical Physics* 80.10 (May 1984), pp. 5095–5106. DOI: 10.1063/1.446581.

[224] D. Babusci, G. Dattoli, and M. Quattromini. "On integrals involving Hermite polynomials". In: (Mar. 2011). arXiv: 1103.1210 [math-ph].

[225] Tommaso Caneva, Tommaso Calarco, and Simone Montangero. "Chopped random-basis quantum optimization". In: *Physical Review A* 84.2 (Aug. 2011), p. 022326. DOI: 10.1103/physreva.84.022326.

[226] Jonathan Keeling. *Light-Matter Interactions and Quantum Optics*. URL: https://www.st-andrews.ac.uk/~jmjk/keeling/teaching/quantum-optics.pdf.

[227] Bharath Srivathsan et al. "Measuring the temperature and heating rate of a single ion by imaging". In: *New Journal of Physics* 21.11 (Nov. 2019), p. 113014. DOI: 10.1088/1367-2630/ab4f43.

[228] S. Knünz et al. "Sub-millikelvin spatial thermometry of a single Doppler-cooled ion in a Paul trap". In: *Physical Review A* 85.2 (Feb. 2012), p. 023427. DOI: 10.1103/physreva.85.023427.

This Ph.D. thesis has been typeset by means of the TEX-system facilities. The typesetting engine was pdfLATEX. The document class was `toptesi`, by Claudio Beccari, with option `tipotesi=scudo`. This class is available in every up-to-date and complete TEX-system installation.